NASA Technical Paper 1154

Solution of Axisymmetric and Two-Dimensional Inviscid Flow Over Blunt Bodies by the Method of Lines

CASE FILE COPY

H. Harris Hamilton II

APRIL 1978

NASA

NASA Technical Paper 1154

Solution of Axisymmetric and Two-Dimensional Inviscid Flow Over Blunt Bodies by the Method of Lines

H. Harris Hamilton II
Langley Research Center
Hampton, Virginia

National Aeronautics
and Space Administration

**Scientific and Technical
Information Office**

1978

SUMMARY

The method of lines (MOL) has been used to obtain solutions to axisymmetric and two-dimensional inviscid flow over smooth blunt bodies. Comparisons with experimental data and the results of other computational methods have demonstrated that very accurate solutions can be obtained by using relatively few lines with this approach. The method is efficient; typical converged solutions have been obtained in 100 to 150 total integrations. The method of lines is semidiscrete and has relatively low core storage requirements as compared with fully discrete methods (such as time-dependent techniques) since very little data are stored across the shock layer. This latter feature is very attractive for three-dimensional problems because it enables computer storage requirements to be reduced by approximately an order of magnitude.

The disadvantage of the method of lines is that roundoff errors increase exponentially with number of lines; thus, the total number of lines that can be used for a particular problem is limited. In the present study it was found that 9 lines was a practical upper limit for two-dimensional and axisymmetric problems. This condition limits application of the method to smooth body geometries where relatively few lines would be adequate to describe changes in the flow variables around the body.

Extension of the method to three dimensions is conceptually straightforward; however, three-dimensional applications would also be limited to smooth body geometries although not necessarily to a total of 9 lines.

INTRODUCTION

Over the past two decades, much effort has been devoted to solving the inviscid flow field over blunt bodies. Two basic approaches have been used: (1) an inverse approach – where the shock wave is given and the body shape and details of the flow within the shock layer are unknown, and (2) a direct approach – where the body is given and all details of the flow within the shock layer are unknown. (See ref. 1.)

For the inverse problem, the steady flow equations are usually solved by marching inward from the known shock wave to obtain the solution for the body. (See refs. 2 to 8.) Since the steady flow equations are of a mixed elliptic-hyperbolic type, this initial value problem is ill posed and inherent instabilities are present which complicate the solution procedure. (See ref. 9.) The inverse problem can be made direct by iteration; however,

it is not always clear how a solution which gives an approximation to a desired body shape is to be improved (ref. 1) and thus solutions for general body shapes may be difficult to obtain. The inverse approach does have two attractive features: (1) solutions are usually very fast; and (2) relatively low computer storage is required, since it is unnecessary to store all flow field data within the shock layer.

More recently, time-dependent finite-difference techniques have been used successfully to solve the more difficult direct problem. (See refs. 10 to 13.) The techniques take advantage of the hyperbolic nature of the unsteady flow equations by marching in time from approximate initial conditions to the desired steady-state solution (asymptotically). This initial value problem is well posed and thus eliminates the instabilities that arise with the inverse approach. In addition, the time-dependent technique can be used to compute the flow field around complicated geometries and the extension to three dimensions is straightforward. (See refs. 14 and 15.) However, these techniques require relatively large computing times and storage, since even when shock fitting is used (refs. 11 and 12), the entire shock layer must be discretized.

Telenin (refs. 16 and 17) has proposed an alternate method of solving the direct blunt body problem called the "method of straight lines" which combines many of the advantages of the inverse approach with the ability to treat more general geometric shapes. This same method has been used to solve nonlinear conical flows in references 18, 19, and 20 wherein it was called the method of lines (MOL).

The purpose of the present paper is to explore the application of the method of lines for computation of the axisymmetric and two-dimensional flow over blunt-nosed bodies immersed in an oncoming supersonic stream at an angle of attack of 0°.

SYMBOLS

A,B,C parameters in equation (30) for body shape

a speed of sound, $\tilde{a}/\tilde{V}_{\infty}$

B_b body bluntness parameter (see eq. (26))

c_p specific heat at constant pressure

c_v specific heat at constant volume

$g,G_1,G_2,\ldots,G_5$ parameters defined by equation (12)

H	total enthalpy, $\bar{H}/\bar{V}_\infty^2$
h	static enthalpy, $\bar{h}/\bar{V}_\infty^2$
j	indicator, $j = 0$ for 2-D flow, $j = 1$ for axisymmetric flow
M	Mach number
n	line number
NETA	number of integration steps from shock to body
NM	number of lines
p	pressure, $\bar{p}/\bar{\rho}_\infty \bar{V}_\infty^2$
$\bar{R}_b$	radius of curvature of nose, m
r,ϕ	polar coordinates (see fig. 1)
t	time, $\bar{V}_\infty \bar{t}/\bar{R}_b$
$\bar{t}$	dimensional time, sec
V	velocity component normal to body, $\bar{V}/\bar{V}_\infty$
V_∞	free-stream velocity, $\bar{V}_\infty/\bar{V}_\infty = 1$
$\bar{V}_\infty$	dimensional free-stream velocity, m/sec
$(v_n)_s$	velocity component normal to shock wave, $(\bar{v}_n)_s/\bar{V}_\infty$
v_r,v_ϕ	velocity components in polar coordinate system (see fig. 1), $\bar{v}_r/\bar{V}_\infty$ and $\bar{v}_\phi/\bar{V}_\infty$
x,y	Cartesian coordinates (see fig. 3), $\bar{x}/\bar{R}_b$, $\bar{y}/\bar{R}_b$
x_p	location of pole of coordinate system (see fig. 3), $\bar{x}_p/\bar{R}_b$

β_s shock wave angle

γ ratio of specific heats, $\bar{c}_p/\bar{c}_v$

γ_0 constant in equation (19b)

Δr local shock-layer thickness (eq. (8))

$\Delta\eta$ integration step size in $-\eta$-direction

$\Delta\xi$ step size in ξ-direction

δ shock standoff perturbation parameter $\left(\text{typically } 10^{-6} \text{ or } 10^{-7}\right)$

ϵ convergence criterion

$\bar{\epsilon}$ criterion for modified iteration procedure

ζ_b angle between tangent to body and line r = Constant

ζ_s angle between tangent to shock wave and line r = Constant

η_r, η_ϕ derivative of η with respect to r and ϕ (eqs. (7a) and (7b))

ξ, η transformed coordinates defined by equation (6)

ξ_r, ξ_ϕ derivatives of ξ with respect to r and ϕ (eqs. (7a) and (7b))

ρ density, $\bar{\rho}/\bar{\rho}_\infty$

Superscripts:

$(\bar{})$ dimensional quantity

$(\tilde{})$ predicted quantity

$(\,)'$ derivative with respect to η in equations (19)

Subscripts:

b	body
s	shock
∞	free stream
n	nth line
max	maximum

METHOD

The problem is to compute the inviscid two-dimensional or axisymmetric flow over a blunt-nosed body immersed in an oncoming supersonic stream. Solutions are to be obtained throughout the subsonic region and downstream into the supersonic region (fig. 1).

Flow Field Equations

The partial differential equations governing the two-dimensional or axisymmetric flow of an inviscid, nonconducting fluid in polar coordinates (fig. 1) are

$$\frac{D\rho}{Dt} + \rho\left(\frac{\partial v_r}{\partial r} + \frac{1}{r}\frac{\partial v_\phi}{\partial \phi} + \frac{j+1}{r}v_r + j\frac{\cot\phi}{r}v_r\right) = 0 \tag{1}$$

$$\frac{Dv_r}{Dt} - \frac{v_\phi^2}{r} + \frac{1}{\rho}\frac{\partial p}{\partial r} = 0 \tag{2}$$

$$\frac{Dv_\phi}{Dt} + \frac{v_r v_\phi}{r} + \frac{1}{r\rho}\frac{\partial p}{\partial \phi} = 0 \tag{3}$$

where

$$\frac{D}{Dt} = \frac{\partial}{\partial t} + v_r\frac{\partial}{\partial r} + \frac{v_\phi}{r}\frac{\partial}{\partial \phi}$$

denotes the substantial derivative and $j = 0$ for two-dimensional flow and $j = 1$ for axisymmetric flow.

Noting that entropy is constant along streamlines leads to the following relation:

$$\frac{1}{a^2}\frac{Dp}{Dt} = \frac{D\rho}{Dt} \tag{4}$$

which can be used to replace the density derivative in equation (1) to obtain the following relationship:

$$\frac{Dp}{Dt} + a^2\rho\left(\frac{\partial v_r}{\partial r} + \frac{1}{r}\frac{\partial v_\phi}{\partial \phi} + \frac{j+1}{r}v_r + j\frac{\cot\phi}{r}v_\phi\right) = 0 \tag{5}$$

Equations (2), (3), and (5) contain derivatives of p, v_r, and v_ϕ only.

Computational Domain

To facilitate integration of this system of partial differential equations, the region (fig. 1) bounded by the stagnation streamline, the bow shock wave, a line $\phi = \phi_{max}$ (located in the supersonic region), and the body surface is mapped into a rectangular domain (fig. 2) using the transformation equations

$$\left.\begin{aligned} \xi &= \frac{\phi}{\phi_{max}} \\ \eta &= \frac{r - r_b(\phi)}{r_s(\phi) - r_b(\phi)} \end{aligned}\right\} \tag{6}$$

From these transformation equations, a set of transformation operators can be defined as

$$\frac{\partial}{\partial r} = \eta_r\frac{\partial}{\partial \eta} + \xi_r\frac{\partial}{\partial \xi} = \frac{1}{\Delta r}\frac{\partial}{\partial \eta} \tag{7a}$$

$$\frac{\partial}{\partial \phi} = \eta_\phi\frac{\partial}{\partial \eta} + \xi_\phi\frac{\partial}{\partial \xi} \tag{7b}$$

where

$$\Delta r = r_s(\phi) - r_b(\phi) \tag{8}$$

which will transform the governing differential equations (2), (3), and (5) into the following system under the condition of steady flow (see appendix A)

$$\frac{\partial p}{\partial \eta} = -\frac{1}{G_1}\left(G_2 \frac{\partial p}{\partial \xi} + G_3 \frac{\partial v_\phi}{\partial \xi} + G_4 \frac{\partial v_r}{\partial \xi} + G_5\right) \tag{9}$$

$$\frac{\partial v_r}{\partial \eta} = -\frac{1}{g}\left[\left(\frac{1}{\rho \Delta r}\right)\frac{\partial p}{\partial \eta} + \left(\frac{v_\phi \xi_\phi}{r}\right)\frac{\partial v_r}{\partial \xi} - \frac{v_\phi^2}{r}\right] \tag{10}$$

$$\frac{\partial v_\phi}{\partial \eta} = -\frac{1}{g}\left[\frac{1}{\rho r}\left(\xi_\phi \frac{\partial p}{\partial \xi} + \eta_\phi \frac{\partial p}{\partial \eta}\right) + \left(\frac{v_\phi \xi_\phi}{r}\right)\frac{\partial v_\phi}{\partial \xi} + \frac{v_r v_\phi}{r}\right] \tag{11}$$

where

$$g = \frac{v_r}{\Delta r} + \frac{v_\phi \eta_\phi}{r} \tag{12a}$$

$$G_1 = g - \frac{a^2}{g}\left[\frac{1}{(\Delta r)^2} + \left(\frac{\eta_\phi}{r}\right)^2\right] \tag{12b}$$

$$G_2 = \frac{\xi_\phi}{r}\left[v_\phi - \frac{a^2}{g}\left(\frac{\eta_\phi}{r}\right)\right] \tag{12c}$$

$$G_3 = \frac{a^2 \rho}{rg}\left(g \xi_\phi - \frac{v_\phi \xi_\phi \eta_\phi}{r}\right) \tag{12d}$$

$$G_4 = -\frac{a^2 \rho}{rg}\left(\frac{v_\phi \xi_\phi}{\Delta r}\right) \tag{12e}$$

$$G_5 = \frac{a^2 \rho}{rg}\left[\frac{v_\phi^2}{\Delta r} + v_r(j+1)g + jg \cot \phi v_\phi - \frac{\eta_\phi v_r v_\phi}{r}\right] \tag{12f}$$

Equations (9) to (11) contain five dependent variables $\left(p,\ \rho,\ a^2,\ v_r, \text{ and } v_\phi\right)$. To solve for these variables, two additional equations are required. The integrated form of the energy equation for an ideal gas is used

$$\frac{p}{\rho}\left(\frac{\gamma}{\gamma - 1}\right) + \frac{v_r^2 + v_\phi^2}{2} = H \tag{13}$$

along with an equation of state for an ideal gas relating a^2, p, and ρ

$$a^2 = \frac{\gamma p}{\rho} \tag{14}$$

Note that equations (13) and (14) are valid for ideal gases only and would have to be replaced by other appropriate equations if equilibrium chemistry were to be considered.

Equation (9) is indeterminant along the stagnation streamline for the case of axisymmetric flow because of the term $(\cot \phi)v_\phi$; thus, it must be replaced by its limiting form along this line. (See appendix B.) For $j = 1$ and $\xi = 0$,

$$\frac{\partial p}{\partial \eta} = -\frac{1}{G_1}\left(2G_3 \frac{\partial v_\phi}{\partial \xi} + \hat{G}_5\right) \tag{15}$$

where

$$\hat{G}_5 = \frac{a^2 \rho}{rg}\left(2gv_r\right) \tag{16}$$

The Method of Lines

The method used to obtain solutions to the present blunt-body problem is patterned after the method presented in reference 19, for the solution of nonlinear conical flow problems, wherein it was called the method of lines (MOL). The application of the method of lines in the present problem proceeds as follows. The region of interest in the ξ,η-plane $(0 \leqq \xi \leqq 1,\ 0 \leqq \eta \leqq 1)$ is divided by NM straight lines parallel to the η-axis (see fig. 2), the line $n = 1$ being coincident with the stagnation streamline in the physical plane and the line $n = NM$ being coincident with the line $\phi = \phi_{max}$ in the physical plane. The boundary $\eta = 0$ represents the body surface and the boundary $\eta = 1$ represents the bow shock wave. This arrangement divides the region in $NM - 1$ strips with the NM lines forming the boundaries of the strips. In the present application, the spacing between lines is equal although this is not an inherent requirement of the method.

At each strip boundary or line, the system of partial differential equations (9) to (11) is reduced to a set of ordinary differential equations by replacing the ξ-derivatives with finite-difference approximations. The resulting system of coupled ordinary differential equations can then be integrated from an assumed bow shock wave to the body surface. This process must be repeated until a bow shock wave is found which yields the correct surface boundary conditions. The problem is formulated as a "direct free boundary problem" which has some features that are obviously similar to the inverse problem described in references 2 to 8.

Finite-difference approximations.- Although several types of finite-difference approximations have been tried, one which approximately takes into account the physical zone of dependence in the flow has been found to yield much more satisfactory results than the other schemes that have been tried. In this scheme, at each step of the integration, when the Mach number at a point on the nth line is subsonic ($M < 1$), a central difference (ref. 21) is used to represent the ξ-derivative. Thus, for $M < 1$, the derivative of some general quantity F becomes

$$\frac{\partial F}{\partial \xi} = \frac{F_{n+1} - F_{n-1}}{2\,\Delta\xi} \tag{17}$$

When the Mach number is supersonic ($M > 1$), a three-point backward difference (ref. 21) is used; thus, for $M \geq 1$

$$\frac{\partial F}{\partial \xi} = \frac{3F_n - 4F_{n-1} + F_{n-2}}{2\,\Delta\xi} \tag{18}$$

Both expressions are formally second order accurate although the first expression has a smaller error term than the second. Using the more accurate central difference formula (eq. (16)) throughout the field has not been found as successful because it allows an improper direct coupling between downstream and upstream points in the supersonic region which slows convergence.

Extension of MOL to three dimensions.- It is conceptually straightforward to extend the method of lines to treat three-dimensional blunt-body problems. For this case, lines would be constructed in a number of meridional planes around the body similar to those constructed in the ξ,η-plane described previously. This procedure would divide the flow field between the shock and the body into a number of regions or "cells" with the lines forming the edges of the cells. Along each line, the system of governing partial differential equations would be reduced to a system of coupled ordinary differential equations by

replacing the partial derivatives in both the longitudinal and circumferential directions by finite-difference approximations similar to those described in the previous section. From this point, the similarity to the two-dimensional or axisymmetric problem should be obvious. The major advantage that the method of lines holds for three-dimensional problems is that flow field data need not be stored at grid points between the shock and the body since a system of ordinary differential equations are integrated from the shock to the body to obtain the solution. This method leads to a reduction in computer storage requirements by approximately an order of magnitude compared with fully discrete methods (such as time-dependent methods) when the entire shock layer must be descretized.

Integration of the ordinary differential equations.- The system of differential equations (9) to (11) is integrated simultaneously along each line with the derivatives on the right-hand side being evaluated from equations (17) and (18). The finite-difference approximations cause the resulting differential equations at each line to be coupled to the differential equations on adjacent lines; thus, the system of differential equations becomes a set of 3NM coupled ordinary differential equations. Of the many methods available for integrating sets of ordinary differential equations (see ref. 22), a two-step predictor-corrector method proposed by Stetter has been used. Following this method, the predictor step is

$$\tilde{F}_n^{\eta-\Delta\eta} = F_n^{\eta} - \frac{\Delta\eta}{2}\left[3(F')_n^{\eta} - (F')_n^{\eta+\Delta\eta}\right] \tag{19a}$$

and the corrector step is

$$F_n^{\eta-\Delta\eta} = \gamma_0 \tilde{F}_n^{\eta-\Delta\eta} - \left(1 - \gamma_0\right)\frac{\Delta\eta}{2}\left[\left(\tilde{F}'\right)_n^{\eta-\Delta\eta} + (F')_n^{\eta}\right] \tag{19b}$$

where γ_0 was taken as 0.65. This method is formally second-order accurate and very stable; however, it is a two-step method and requires some other starting solution to compute the first step. In the present study, a simple Euler-predictor trapezoidal corrector was used to start the integration and equal size steps were taken in the η-direction throughout the entire integration cycle. Typically 5 to 10 integration steps were taken between the shock and the body.

Symmetry and Boundary Conditions

The flow is symmetric about the stagnation streamline; thus, symmetry conditions are imposed along the line $\xi = 0$ $(\eta = 1)$

$$v_\phi = \frac{\partial p}{\partial \xi} = \frac{\partial v_r}{\partial \xi} = 0 \tag{20}$$

At the start of each integration cycle, the shock jump relations are used to determine all properties on the downstream side of the shock wave at $\eta = 1$. (See appendix C.) The initial shock wave shape is assumed and then iterated until the surface boundary conditions are satisfied. The procedure used to correct the shock shape during the iteration process is described in a subsequent section.

Along the body surface, the normal component of velocity must vanish. Thus, at the body surface $(\eta = 0)$ the following relation must hold:

$$V_b = v_r \cos \zeta_b - v_\phi \sin \zeta_b = 0 \tag{21}$$

The shock wave shape is initially assumed and iterated upon until this boundary condition is satisfied on each line.

The downstream boundary $(\xi = 1)$ must be chosen so that at this boundary the flow is totally supersonic, and on this boundary three-point backward differencing is used. (See eq. (18).)

Determination of Shock Wave Shape

The iteration procedure for determining the shock wave shape is the same as that used in reference 19 for conical flows. The shape of the assumed shock wave is given by the known numerical function $r(\eta = 1, \xi) = r_s(\xi)$; thus, this function can be differentiated numerically, using either equation (17) or (18), to determine $dr_s/d\xi$. Knowing $r_s(\xi)$ and $dr_s/d\xi$ at each line allows the flow properties $\left(p,\ \rho,\ a^2,\ v_r, \text{ and } v_\phi\right)$ on the downstream side of the bow shock wave to be determined from the shock jump relations. (See appendix C.) These flow properties can be used to evaluate the right-hand side of equations (9) to (11) to start the numerical integration procedure at $\eta = 1$ and proceed inward toward the body surface $(\eta = 0)$. Only the correct shock shape will satisfy the surface boundary conditions (eq. (21)). A corrective procedure must be used to drive the shock shape in a direction that will eventually satisfy these boundary conditions at the body surface.

Newton iteration for shock shape.- The shock wave is given by the equation

$$r_s(\xi) = r_b(\xi) + \Delta r(\xi) \tag{22}$$

Since the body shape $r_b(\xi)$ is always known (direct problem), the shock shape is expressed numerically by a set of NM shock-layer thicknesses Δr_n, one for each line. For each line, there is a normal component of velocity at the surface $(V_b)_n$. A Newton-type iteration procedure will be used for correcting the NM values of Δr_n so that

$$\max\left|(V_b)_n\right| \leqq \epsilon$$

where ϵ is a small prespecified convergence criterion $\left(\text{typically } \epsilon = 10^{-3}\right)$. The steps in the procedure are as follows:

(1) Obtain an initial set of values for Δr_n either from experience or from a solution to a previous problem.

(2) Determine properties on the downstream side of the shock wave at each line.

(3) Use the results of step (2) as initial conditions to start the numerical integration of the system of ordinary differential equations from the shock to the body surface and evaluate V_b at each line.

(4) Determine $\max\left|(V_b)_n\right|$. If $\max\left|(V_b)_n\right| \leqq \epsilon$, the solution is considered converged; if not, proceed to step (5).

(5) Successively perturb the value of the shock-standoff distance Δr_n at each line to $(1 + \delta)\Delta r_n$, where δ is a small number $\left(\text{typically } \delta = 10^{-6} \text{ or } 10^{-7}\right)$, and repeat steps (2) to (4). This procedure results in a small change in $(V_b)_n$ with each perturbation that can be related to a change in the shock-layer thickness at each line

$$\frac{\partial(V_b)_n}{\partial(\Delta r_j)} \qquad (n = 1,2,3,\ldots,NM)$$

After completion of the NM perturbations, a NM × NM matrix of "influence coefficients" is generated which can be used to correct the shock shape in a way so that $(V_b)_n$ will be driven toward zero.

(6) Solve the first-order linear system

$$\sum_{j=1}^{NM} \frac{\partial(V_b)_n}{\partial(\Delta r_j)} \Delta(\Delta r_j) = -(V_b)_n \qquad (n = 1,2,3,\ldots,NM) \tag{23}$$

to obtain the corrections $\Delta(\Delta r_j)$ to the value of the shock-layer thickness at each line which will tend to drive $(V_b)_n$ toward zero.

(7) By using the new shock shape

$$(\Delta r_n)_{new} = (\Delta r_n)_{old} + \Delta(\Delta r_n) \tag{24}$$

begin a new cycle at step (2) and continue until the test at step (4) is satisfied. Note that each complete cycle requires one initial integration and NM perturbations (or NM + 1 integrations).

In reference 19, it was shown that a modified Newton iteration procedure could often be used to greatly speed up the convergence process. In this procedure, when $\max\left|(V_b)_n\right| \leq \bar{\epsilon}$ (where $\bar{\epsilon}$ is a small number, usually around 0.02 to 0.05), the perturbations were eliminated and the corrections to the shock-layer thickness at each line $\Delta(\Delta r_n)$ were evaluated from the matrix of old influence coefficients. This procedure reduces the number of integrations per cycle by NM and although it generally requires more cycles, it will usually require fewer total number of integrations (and thus less work) to obtain a converged solution.

Initial shock shape.- The ability to obtain a converged solution for certain body shapes and flow conditions depends strongly upon the accuracy of the initial guess for the shock shape. However, for a sphere (or circular cylinder) and a paraboloid at moderately large Mach number $(M_\infty > 5)$, converged solutions can usually be obtained by starting with a shock shape represented by a constant shock-layer thickness Δr_n at each line. By using the solution thus obtained, it is usually easy to "build" the solution for other desired body shapes or flow conditions with the procedure outlined as follows.

(1) A converged solution is obtained for a problem similar to the desired problem but differing in some parameter F where F could represent M_∞, γ, or B_b. See section on body geometry.

(2) A small change is made in F and a new solution is computed for $F_{new} = F_{old} + \Delta F$. The initial value of ΔF is usually very small so that the old shock shape is a good approximation to the shock shape for the new case.

(3) The changes in the shock-layer thickness Δr_n are obtained at each line between the new and old case and the derivative $d\,\Delta r_n/dF$ is computed numerically.

(4) A new set of approximate shock-layer thicknesses are obtained from the assumed linear relationship

$$(\Delta r_n)_{new} = (\Delta r_n)_{old} + \left(\frac{\partial\, \Delta r_n}{\partial F}\right) \Delta F \tag{25}$$

and a solution is computed for a new value of the parameter $F_{new} = F_{old} + \Delta F$ by using the shock shape obtained from equation (25) as an initial guess.

(5) Steps (3) and (4) are then repeated until the desired problem has been solved. This procedure is easily adapted to automatic computation and is very efficient since it insures that the initial guess at the shock shape is a reasonably good approximation. This procedure has been built into the present computer program and is used extensively for obtaining solutions to the more difficult problems.

Determination of Surface Properties

From equations (9) to (11), it should be observed that if g or G_1 becomes zero, a singularity occurs in the differential equations so that the numerators of equations (9) to (11) must also become zero if the η-derivatives are to remain finite. Numerically, evaluation of the η-derivatives becomes very difficult when g or G_1 becomes small and the integration process must be stopped at this point. When the assumed shock shape is far from the converged shock shape, it may not be possible to integrate the differential equations all the way to the body surface without a singularity of the type mentioned above occurring. When this happens, the velocity components normal to the body

$$V = v_r \cos \zeta_b - v_\phi \sin \zeta_b$$

are extrapolated to the surface along each line by using a second-order accurate extrapolation technique which yields values of $(V_b)_n$ that can be used to correct the shock shape for successive iterations. As the shock shape approaches convergence, this type of singularity generally does not occur (if the last line does not extend too far into the supersonic region) and the integration of the differential equations can proceed to the surface.

In evaluating flow properties on the surface, only the predictor step (eq. (19a)) in the numerical integration routine is used since the equations for the η-derivatives (eqs. (9) to (11)) are singular at $\xi = 0$. However, the predictor step is second order accurate and thus the results at the body surface have the same formal order of accuracy as the results away from the body surface.

BODY GEOMETRY

The body geometries that are considered in the present paper have a projection in the $\bar{x},\bar{y}$ plane that is described by the equation for a general conic section

$$\bar{y}^2 = 2\bar{R}_b\bar{x} - B_b\bar{x}^2 \tag{26}$$

where $\bar{R}_b$ is the radius of curvature at $\bar{x} = 0$ and B_b is a bluntness parameter. This equation can be placed in a more convenient form if $\bar{x}$ and $\bar{y}$ are nondimensionalized by dividing by the radius of curvature $\bar{R}_b$. Thus,

$$y^2 = 2x - B_b x^2 \tag{27}$$

The bluntness parameter B_b characterizes the eccentricity of the conic section. Its significance is better understood if it is noted that $B_b < 0$ generates a hyperbola, $B_b = 0$ generates a parabola, and $B_b > 0$ generates an ellipse, with $B_b = 1$ for the special case of a circle. For an ellipse, B_b is related to the ratio of major to minor axes (b/a) by the relation

$$B_b = \left(\frac{b}{a}\right)^2 \tag{28}$$

An axisymmetric body is generated by revolving the curve described by equation (27) about the x-axis. By using the following equations to define x and y (see fig. 3),

$$\left.\begin{aligned} x &= x_p - r\cos\phi \\ y &= r\sin\phi \end{aligned}\right\} \tag{29}$$

an equation for a general conic in polar coordinates is obtained

$$r = \frac{-B + \sqrt{B^2 - 4AC}}{2A} \tag{30}$$

where

$$A = \sin^2\phi + B_b\cos^2\phi$$

$$B = 2\cos\phi\left(1 - B_b x_p\right)$$

$$C = x_p\left(B_b x_p - 2\right)$$

For the results presented in this paper, when $B_b > 0$, x_p is taken as

$$x_p = \frac{1}{B_b} \tag{31}$$

which places the pole of the coordinate system at the point of intersection of the major and minor axes of an ellipse. (See fig. 3.) When $B_b \leq 0$, x_p is set equal to 1 which places the pole of the coordinate system at the center of curvature of the nose.

Thus, equation (30) is very convenient for describing the body shape since a wide variety of bodies can be obtained by varying a single parameter B_b.

RESULTS AND DISCUSSION

In this section, results of computations by the method of lines (MOL) for several smooth body shapes are compared with experimental data and the results of other computational techniques to demonstrate the accuracy and utility of the present method.

Sphere

Pressure distributions over a sphere for $\gamma = 1.4$ are presented in figure 4 for free-stream Mach numbers of 2, 3, 4, 6.05, and 8.06. For each case 9 lines were used and 10 equally sized integration steps were taken between the shock and the body. Experimental data from references 23 and 24 and computed results from reference 5 are presented for comparison. The pressures computed by the MOL agree well with the experimental data for each Mach number considered. The computed results from reference 5 (using an inverse method) agree with the other data in the stagnation region, but underpredict the pressure as the sonic line on the body is approached ($\phi \approx 41^\circ$ to 48°), particularly at low Mach numbers.

The shock-layer thicknesses for these cases are compared in figure 5, where it is seen that for $M_\infty > 3$, the shock-layer thickness predicted by the MOL agrees closely with those from the other data. For $M_\infty = 2$, the MOL predicts a slightly thicker shock layer (by as much as 6 percent when compared with the experimental data of ref. 23); however, the predicted surface pressures were found to agree with the experimental data. (See fig. 4(a).) Since the shock-layer thickness changes rapidly at low Mach numbers, this behavior could easily be due to a small change in the effective Mach number for the tests which would change the shock-layer thickness but have little effect on the measured pressure distribution.

Experience gained through application of the MOL to flow over a sphere and other body shapes indicates that for $\gamma = 1.4$, $M_\infty = 2$ represents a practical lower limit for

using the method. Although solutions can be obtained at slightly lower Mach numbers, the computations become tedious and require more "art than science" to be successful. In references 19 and 20 it was pointed out that when the MOL is applied to Laplace's equation, roundoff errors grow exponentially like $10^{-j} \exp(NX)$ where j is the number of decimal figures in a computation, N is the number of lines, and X is distance along a line from the initial data line. Since the physical shock-layer thickness grows rapidly with decreasing Mach number (for Mach numbers approaching 1), it should be expected that this inaccuracy would lead to convergence problems as the Mach number is reduced. This has been found to be the case in the present study.

For the $M_\infty = 8.06$ condition, a matrix of solutions have been computed by using 5, 7, 9, or 11 lines; 5 or 10 integration steps between the shock and the body; and a full or modified Newton iteration scheme. The results obtained from these computations are compared in tables I, II, and III. Table I lists the conditions for the 16 cases and some results including number of global iterations required for convergence, total number of integrations, and computational time on a CDC CYBER 175 computer for each case. Table II lists the pressures on the body for the ϕ locations associated with the solution for nine lines and table III lists the shock-layer thickness for these same ϕ locations. In tables II and III, results are presented only for the full Newton iteration scheme since there is almost no difference between those and the results for the modified iteration scheme. All solutions were for $\phi_{max} = 45^\circ$ and were started with a constant shock-layer thickness $\Delta r = 0.140$ at each line (concentric shock).

Note first that the results obtained with the modified iteration scheme $(\bar{\epsilon} > \epsilon$, cases 9 to 16$)$ in general required more global iterations but fewer total integrations than with the full Newton iteration scheme $(\bar{\epsilon} = \epsilon$, cases 1 to 8$)$. Since the actual amount of work involved in obtaining a solution is directly proportional to the total number of integrations, the modified iteration scheme required less computer time. However, the reduction in computer time is relatively small (of the order of 10 percent or less) and, in general, has not been found to be large enough to offset the disadvantage that for some problems the modified iteration scheme does not converge. Thus, the full Newton iteration scheme has been used exclusively in the remainder of this paper.

With 11 lines, when 10 steps were taken between the shock and the body (case 1), the solution did not converge. When 5 steps were taken (case 5), the solution passed the convergence criterion, but the entropy on the surface was not constant near the last line and indicated a poor solution. The pressure on the surface at the last line is too high (table II) even though the shock-layer thickness is approximately correct (table III). As discussed previously, roundoff errors grow exponentially with the number of lines so that as the number of lines is increased, it becomes more difficult to obtain a good converged solution. From experience, it has been found that 9 is a practical upper limit for the

number of lines. Some solutions have been obtained with more lines, but the computations become tedious. For all cases, the last line cannot extend too far into the supersonic region, but when the number of lines becomes large, the placement of the last line relative to the sonic line (which is not known a priori) becomes critical.

By comparing the results in tables II and III, it is seen that the solutions to the present problem with as few as 5 lines and 5 steps between the shock and the body are very accurate. In general, it has been found that using up to 9 lines with 5 to 10 integration steps between the shock and the body provides very accurate results for most smooth blunt-body problems considered here.

In figure 6, constant-density lines are presented for flow over a sphere in nitrogen with $M_\infty = 5.017$ along with experimental data from reference 25 and computed results from reference 7. The results computed by MOL are in excellent agreement with those of reference 7 and reasonably good agreement with the experimental data except in the stagnation region where because of the uniformity of the flow, accurate measurements are very difficult to obtain.

In figure 7, constant-density lines are presented for flow over a sphere in argon at $M_\infty = 5.329$ along with experimental data from reference 25 and computed results from reference 7. There is excellent agreement with the computed results of reference 7, but the agreement with the experimental data is poor. The reason for the disagreement with the experimental data is not known; however, the good agreement with the computed results of reference 7 supports the accuracy of the present method.

The MOL was one of several computational methods used in reference 26 to compare with experimental shock shapes over a sphere covering a density ratio across the normal shock from 4 to 19. These density ratios represent a range of effective γ's from 1.667 to 1.067. In that report, it was shown that the results obtained by the MOL agreed well with the experimental shock shapes and with most of the shock shapes predicted by the other computational methods.

Paraboloid

Solutions for the pressure distribution over a paraboloid with $\gamma = 1.4$ are presented in figure 8 for Mach numbers of 10 and 3. Computed results from reference 5 are included for comparison. The solutions agree very closely except in the vicinity of the outflow boundary (ϕ_{max}) where the two solutions deviate slightly. These are typical for the comparisons presented previously for a sphere (see fig. 4) except that for a sphere, experimental data were also available which substantiated the MOL results.

The variations of shock-layer thickness with ϕ for these cases are compared in figure 9. The shock-layer thicknesses for the two solutions agree very closely.

Ellipsoid

Pressure distributions for an ellipsoid with $b/a = 0.5$ and $\gamma = 1.4$ are presented in figure 10 for Mach numbers of 8.06, 6.05, and 4. Experimental data from reference 23 are included for comparison. The computed results agree very closely with the experimental data for each Mach number.

Pressure distributions for an ellipsoid with $b/a = 1.5$ and $\gamma = 1.4$ are presented in figure 11 for Mach numbers of 8.06, 6.05, 4.0, and 3.0 along with experimental data from reference 23. The computed pressure distributions agree closely with the experimental data. The variations of shock-layer thickness with ϕ for this body shape are presented in figure 12 for Mach numbers of 8.06 and 3.0 where it is seen that the MOL results agree closely with the experimental data.

In figure 13, the shock standoff distance at the stagnation point is presented for a body bluntness parameter $B_b = (b/a)^2$ ranging from 0 (paraboloid) to 9 (3:1 ellipsoid) for $M_\infty = 10$, 6, and 3. The only data available for comparison are the computed results from reference 7 which cover a limited range of B_b and M_∞. The shock standoff distances computed by the MOL compare well with the available data from reference 7. This figure illustrates the wide range of body shapes for which the MOL can be applied.

Circular Cylinder

Results for the two-dimensional flow over a circular cylinder are presented in figures 14 and 15 for Mach numbers of 8.06 and 3.0. Figure 14 presents MOL surface pressure distributions compared with experimental data from reference 23 and computed results from reference 6 (inverse method) and from a perfect gas version of the method presented in reference 27 (time-dependent method). The MOL results are in good agreement with those of the other data.

Figure 15 presents MOL shock-layer thicknesses compared with the computed results from reference 6 and the method of reference 27. Experimental data for the shock-layer thicknesses for this case are not available. All results agree well at $M_\infty = 8.06$. At $M_\infty = 3$, there are much larger differences among the results. The results computed by MOL and the method of reference 27 are in reasonably good agreement, but the shock-layer thicknesses from reference 6 are much smaller. Whatever the reason for the differences in the shock-layer thicknesses, the pressures on the surface are unaffected. (See fig. 14(b).)

CONCLUDING REMARKS

The method of lines (MOL) has been used to obtain solutions to axisymmetric and two-dimensional inviscid flow over smooth blunt bodies. Comparisons with experimental

data and the results of other computational methods have demonstrated that very accurate solutions can be obtained by using relatively few lines with this approach. The method is efficient; typical converged solutions have been obtained in 100 to 150 total integrations. The method of lines is semidiscrete and has relatively low core storage requirements as compared with fully discrete methods (such as time-dependent techniques) since very little data are stored across the shock layer. This latter feature is very attractive for three-dimensional problems because it enables core storage requirements to be reduced by approximately an order of magnitude.

The disadvantage of the method of lines is that roundoff errors increase exponentially with number of lines; thus, the total number of lines that can be used for a particular problem is limited. In the present study it was found that 9 lines was a practical upper limit for two-dimensional and axisymmetric problems. This limits application of the method to smooth body geometries where relatively few lines would be adequate to describe changes in the flow variables around the body.

Extension of the method to three dimensions is conceptually straightforward; however, three-dimensional application would also be limited to smooth body geometries although not necessarily to a total of 9 lines.

Langley Research Center
National Aeronautics and Space Administration
Hampton, VA 23665
January 27, 1978

APPENDIX A

TRANSFORMATION OF FLOW FIELD EQUATIONS

Consider the transformation of the flow field equations from physical space (r,ϕ) to the computational space (η,ξ). The flow field equations in physical space (eqs. (2), (3), and (5)) can be written in the following expanded form for steady flow:

$$v_r \frac{\partial v_r}{\partial r} + \frac{v_\phi}{r} \frac{\partial v_r}{\partial \phi} - \frac{v_\phi^2}{r} + \frac{1}{\rho} \frac{\partial p}{\partial r} = 0 \tag{A1}$$

$$v_r \frac{\partial v_\phi}{\partial r} + \frac{v_\phi}{r} \frac{\partial v_\phi}{\partial \phi} + \frac{v_r v_\phi}{r} + \frac{1}{\rho r} \frac{\partial p}{\partial \phi} = 0 \tag{A2}$$

$$v_r \frac{\partial p}{\partial r} + \frac{v_\phi}{r} \frac{\partial p}{\partial \phi} + a^2 \rho \left(\frac{\partial v_r}{\partial r} + \frac{1}{r} \frac{\partial v_\phi}{\partial \phi} + \frac{j+1}{r} v_r + j \frac{\cot \phi}{r} v_\phi \right) = 0 \tag{A3}$$

Using the transformation operators defined by equation (7), equation (A1) transforms as follows:

$$v_r \left(\frac{1}{\Delta r} \frac{\partial v_r}{\partial \eta} \right) + \frac{v_\phi}{r} \left(\eta_\phi \frac{\partial v_r}{\partial \eta} + \xi_\phi \frac{\partial v_r}{\partial \xi} \right) - \frac{v_\phi^2}{r} + \frac{1}{\rho} \left(\frac{1}{\Delta r} \frac{\partial p}{\partial \eta} \right) = 0 \tag{A4}$$

which after solving for $\partial v_r / \partial \eta$ yields equation (10)

$$\frac{\partial v_r}{\partial \eta} = -\frac{1}{g} \left(\frac{1}{\Delta r \rho} \frac{\partial p}{\partial \eta} + \frac{v_\phi \xi_\phi}{r} \frac{\partial v_r}{\partial \xi} - \frac{v_\phi^2}{r} \right) \tag{A5}$$

Similarly, equation (A2) transforms as follows:

$$v_r \left(\frac{1}{\Delta r} \frac{\partial v_\phi}{\partial \eta} \right) + \frac{v_\phi}{r} \left(\eta_\phi \frac{\partial v_\phi}{\partial \eta} + \xi_\phi \frac{\partial v_\phi}{\partial \xi} \right) + \frac{v_r v_\phi}{r} + \frac{1}{\rho r} \left(\eta_\phi \frac{\partial p}{\partial \eta} + \xi_\phi \frac{\partial p}{\partial \xi} \right) = 0 \tag{A6}$$

which after solving for $\partial v_\phi / \partial \eta$ yields equation (11)

$$\frac{\partial v_\phi}{\partial \eta} = -\frac{1}{g}\left[\frac{1}{\rho r}\left(\xi_\phi \frac{\partial p}{\partial \xi} + \eta_\phi \frac{\partial p}{\partial \eta}\right) + \left(\frac{v_\phi \xi_\phi}{r}\right)\frac{\partial v_\phi}{\partial \xi} + \frac{v_r v_\phi}{r}\right] \tag{A7}$$

Finally, equation (A3) transforms as follows:

$$v_r\left(\frac{1}{\Delta r}\frac{\partial p}{\partial \eta}\right) + \frac{v_\phi}{r}\left(\eta_\phi \frac{\partial p}{\partial \eta} + \xi_\phi \frac{\partial p}{\partial \xi}\right) + a^2\rho\left[\frac{1}{\Delta r}\frac{\partial v_r}{\partial \eta} + \frac{1}{r}\left(\eta_\phi \frac{\partial v_\phi}{\partial \eta} + \xi_\phi \frac{\partial v_\phi}{\partial \xi}\right)\right.$$

$$\left. + \frac{j+1}{r} v_r + j \frac{\cot \phi}{r} v_\phi\right] = 0 \tag{A8}$$

Now substituting these expressions for $\partial v_r / \partial \eta$ and $\partial v_\phi / \partial \eta$ and solving for $\partial p / \partial \eta$ yields equation (9)

$$\frac{\partial p}{\partial \eta} = -\frac{1}{G_1}\left(G_2 \frac{\partial p}{\partial \xi} + G_3 \frac{\partial v_\phi}{\partial \xi} + G_4 \frac{\partial v_r}{\partial \xi} + G_5\right)$$

Note that g, G_1, G_2, G_3, G_4, and G_5 are given by equations (12).

APPENDIX B

LIMITING FORM OF FLOW FIELD EQUATIONS ON STAGNATION LINE

For axisymmetric flow equation (9)

$$\frac{\partial p}{\partial \eta} = -\frac{1}{G_1}\left(G_2 \frac{\partial p}{\partial \xi} + G_3 \frac{\partial v_\phi}{\partial \xi} + G_4 \frac{\partial v_r}{\partial \xi} + G_5\right)$$

is indeterminant along the stagnation streamline. Thus, a limiting form of this equation must be derived. Symmetry conditions apply along the stagnation streamline; thus,

$$v_\phi = \frac{\partial p}{\partial \xi} = \frac{\partial v_r}{\partial \xi} = \eta_\phi = 0 \qquad (\xi = 0)$$

Applying these conditions to this equation yields

$$\frac{\partial p}{\partial \eta} = -\frac{1}{G_1}\left(G_3 \frac{\partial v_\phi}{\partial \xi} + G_5\right) \tag{B1}$$

where

$$G_1 = g - \frac{a^2}{g}\left[\frac{1}{(\Delta r)^2}\right] \tag{B2}$$

$$G_3 = \frac{a^2 \rho}{rg}\left(g \xi_\phi\right) \tag{B3}$$

and

$$G_5 = \frac{a^2 \rho}{rg}\left(2 v_r g + g \cot \phi \, v_\phi\right) \tag{B4}$$

The term $\cot \phi \, v_\phi$ in the expression for G_5 is indeterminant along the stagnation streamline ($\xi = 0$); thus, the limiting form of this expression must be used

$$\lim_{\phi \to 0} \cot \phi \, v_\phi = \frac{\partial v_\phi}{\partial \phi} = \xi_\phi \frac{\partial v_\phi}{\partial \xi} \tag{B5}$$

By using this result, equation (B4) becomes

$$G_5 = \frac{a^2 \rho}{rg}\left(2v_r g + g\xi_\phi \frac{\partial v_\phi}{\partial \xi}\right)$$

$$= \frac{a^2 \rho}{rg}\left(g\xi_\phi\right)\frac{\partial v_\phi}{\partial \xi} + \frac{a^2 \rho}{rg}\left(2v_r g\right)$$

$$= G_3 \frac{\partial v_\phi}{\partial \xi} + \hat{G}_5 \tag{B6}$$

where

$$\hat{G}_5 = \frac{a^2 \rho}{rg}\left(2v_r g\right) \tag{B7}$$

Substituting equation (B6) into equation (B1) yields equation (15)

$$\frac{\partial p}{\partial \eta} = -\frac{1}{G_1}\left(2G_3 \frac{\partial v_\phi}{\partial \xi} + \hat{G}_5\right) \qquad (\xi = 0)$$

which is determinate along the stagnation streamline for axisymmetric flow.

APPENDIX C

SHOCK JUMP CONDITIONS

Consider the flow at the bow shock wave depicted in sketch (a).

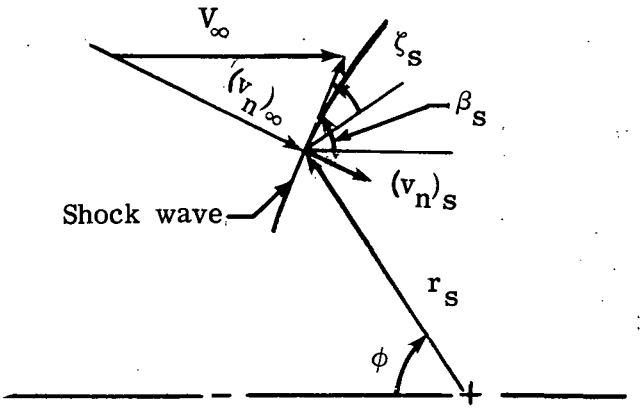

Sketch (a)

The shock wave angle β_s is given by the equation:

$$\beta_s = \frac{\pi}{2} - \phi + \zeta_s \tag{C1}$$

where

$$\zeta_s = \tan^{-1}\left(\frac{1}{r_s}\frac{dr_s}{d\phi}\right) = \tan^{-1}\left(\frac{1}{r_s}\xi_\phi\frac{dr_s}{d\xi}\right) \tag{C2}$$

The polar velocity components at the shock wave are given by the equations

$$\left(v_r\right)_s = -\left(v_n\right)_s \cos\zeta_s + V_\infty \cos\beta_s \sin\zeta_s \tag{C3}$$

$$\left(v_\phi\right)_s = \left(v_n\right)_s \sin\zeta_s + V_\infty \cos\beta_s \cos\zeta_s \tag{C4}$$

The oblique shock wave relations can be written in the form (ref. 28)

$$\rho_\infty V_\infty \sin\beta_s = \rho_s\left(v_n\right)_s \tag{C5}$$

$$p_\infty + \rho_\infty V_\infty^2 \sin^2\beta_s = p_s + \rho_s \left(v_n\right)_s^2 \tag{C6}$$

$$h_\infty + \frac{V_\infty^2 \sin^2\beta_s}{2} = h_s + \frac{\left(v_n\right)_s^2}{2} \tag{C7}$$

The nondimensional free-stream variables have the following values:

$$\left.\begin{aligned} V_\infty &= \rho_\infty = 1 \\ h_\infty &= \frac{1}{(\gamma - 1)M_\infty^2} \\ p_\infty &= \frac{1}{\gamma M_\infty^2} \end{aligned}\right\} \tag{C8}$$

and for a perfect gas the density on the downstream side of the shock wave is given by the following equation:

$$\rho_s = \frac{(\gamma + 1)M_\infty^2 \sin^2\beta_s}{(\gamma - 1)M_\infty^2 \sin^2\beta_s + 2} \tag{C9}$$

Thus, knowing γ and M_∞ and the shock wave angle β_s, which can be determined from equations (C1) and (C2), the properties on the downstream side of the shock wave $\left(v_n\right)_s$, p_s, and h_s can be calculated from equations (C5), (C6), and (C7). Finally, $\left(v_r\right)_s$ and $\left(v_\phi\right)_s$ are calculated from equations (C3) and (C4).

REFERENCES

1. Hayes, Wallace D.; and Probstein, Ronald F.: Hypersonic Flow Theory. Volume I – Inviscid Flows. Second ed., Academic Press, Inc., 1966.

2. Zlotnick, Martin; and Newman, Donald J.: Theoretical Calculation of the Flow on Blunt-Nosed Axisymmetric Bodies in a Hypersonic Stream. RAD-TR-2-57-29 (Contract No. AF-04(645)-30), AVCO Res. and Advanced Dev. Div., Sept. 19, 1957.

3. Mangler, K. W.: The Calculation of the Flow Field Between a Blunt Body and the Bow Wave. Hypersonic Flow, A. R. Collar and J. Tinkler, eds., Academic Press, Inc., 1960, pp. 219-237.

4. Vaglio-Laurin, Roberto; and Ferri, Antonio: Theoretical Investigation of the Flow Field About Blunt-Nosed Bodies in Supersonic Flight. J. Aero/Space Sci., vol. 25, no. 12, Dec. 1958, pp. 761-770.

5. Van Dyke, Milton D.; and Gordon, Helen D.: Supersonic Flow Past a Family of Blunt Axisymmetric Bodies. NASA TR R-1, 1959.

6. Fuller, Franklyn B.: Numerical Solutions for Supersonic Flow of an Ideal Gas Around Blunt Two-Dimensional Bodies. NASA TN D-791, 1961.

7. Lomax, Harvard; and Inouye, Mamoru: Numerical Analysis of Flow Properties About Blunt Bodies Moving at Supersonic Speeds in an Equilibrium Gas. NASA TR R-204, 1964.

8. Webb, H. G., Jr.; Dresser, H. S.; Adler, B. K.; and Waiter, S. A.: Inverse Solution of Blunt-Body Flowfields at Large Angle of Attack. AIAA J., vol. 5, no. 6, June 1967, pp. 1079-1085.

9. Hadamard, Jacques: Lectures on Cauchy's Problem in Linear Partial Differential Equations. Yale Univ. Press (New Haven), 1923. (Also available as Dover Publ., Inc., c.1952.)

10. Bohachevsky, Ihor O.; and Rubin, Ephraim L.: A Direct Method for Computation of Nonequilibrium Flows With Detached Shock Waves. AIAA J., vol. 4, no. 4, Apr. 1966, pp. 600-607.

11. Moretti, Gino; and Abbett, Michael: A Time-Dependent Computational Method for Blunt Body Flows. AIAA J., vol. 4, no. 12, Dec. 1966, pp. 2136-2141.

12. Barnwell, Richard W.: A Time-Dependent Method for Calculating Supersonic Blunt-Body Flow Fields With Sharp Corners and Embedded Shock Waves. NASA TN D-6031, 1970.

13. Taylor, T. D.: Numerical Methods for Predicting Subsonic, Transonic and Supersonic Flow. AGARDograph No. 187, Jan. 1974.

14. Moretti, Gino; and Bleich, Gary: Three-Dimensional Flow Around Blunt Bodies. AIAA J., vol. 5, no. 9, Sept. 1967, pp. 1557-1562.

15. Barnwell, Richard W.: A Time-Dependent Method for Calculating Supersonic Angle-of-Attack Flow About Axisymmetric Blunt Bodies With Sharp Shoulders and Smooth Nonaxisymmetric Blunt Bodies. NASA TN D-6283, 1971.

16. Belotserkovskiy, O. M., ed.: Numerical Methods for Solving Problems of Mechanics of Continuous Media. NASA TT F-667, 1972.

17. Gilinskiy, S. M.; Telenin, G. F.; and Tinyakov, G. P.: A Method of Calculating Supersonic Flow Around Blunted Bodies With Detached Shock Waves. NASA TT F-13026, 1970.

18. Jones, D. J.: Numerical Solutions of the Flow Field for Conical Bodies in a Supersonic Stream. Aeronaut. Rep. LR-507 (NRC No. 10361), Nat. Res. Counc. Can. (Ottawa), July 1968.

19. Klunker, E. B.; South, Jerry C., Jr.; and Davis, Ruby M.: Calculation of Nonlinear Conical Flows by the Method of Lines. NASA TR R-374, 1971.

20. Jones, D. J.; South, J. C., Jr.; and Klunker, E. B.: On the Numerical Solution of Elliptic Partial Differential Equations by the Method of Lines. J. Comput. Phys., vol. 9, no. 3, June 1972, pp. 496-527.

21. Salvadori, Mario G.; and Baron, Melvin L.: Numerical Methods in Engineering. Prentice-Hall, Inc., 1961.

22. Lapidus, Leon; and Seinfeld, John H.: Numerical Solution of Ordinary Differential Equations. Academic Press, Inc., c.1971.

23. Belotserkovskiy, O. M., ed.: Supersonic Gas Flow Around Blunt Bodies – Theoretical and Experimental Investigations. NASA TT F-453, 1967.

24. Baer, A. L.: Pressure Distributions on a Hemisphere Cylinder at Supersonic and Hypersonic Mach Numbers. AEDC TN-61-96, U.S. Air Force, Aug. 1961.

25. Sedney, R.; and Kahl, G. D.: Interferometric Study of the Hypersonic Blunt Body Problem. Planetary and Space Science, Vol. 4, Pergamon Press, Inc., 1961, pp. 337-351.

26. Miller, Charles G., III: A Comparison of Measured and Predicted Sphere Shock Shapes in Hypersonic Flows With Density Ratios From 4 to 19. NASA TN D-8076, 1975.

27. Sutton, Kenneth: Characteristics of Coupled Nongray Radiating Gas Flows With Ablation Product Effects About Blunt Bodies During Planetary Entries. Ph.D. Thesis, North Carolina State Univ., 1973. (Available as NASA TM X-72078.)

28. Liepmann, H. W.; and Roshho, A.: Elements of Gasdynamics. John Wiley & Sons, Inc., c.1957.

TABLE I.- CONDITIONS FOR TEST CASES

$[M_\infty = 8.06;\ \gamma = 1.4;\ \phi_{max} = 45^o]$

Case	NM	NETA	ϵ	$\bar{\epsilon}$	Iterations	Integrations	Time, sec
1	11	10	0.001	0.001	No convergence		----
2	9	↓	↓	↓	17	170	7.123
3	7	↓	↓	↓	16	128	4.349
4	5	10	↓	↓	13	78	2.031
*5	11	5	↓	↓	8	96	2.623
6	9	↓	↓	↓	10	100	2.268
7	7	↓	↓	↓	10	80	1.486
8	5	5	↓	.001	10	60	.862
9	11	10	↓	.05	No convergence		----
10	9	↓	↓	↓	21	156	6.564
11	7	↓	↓	↓	21	126	4.313
12	5	10	↓	↓	17	72	1.866
*13	11	5	↓	↓	11	77	2.239
14	9	↓	↓	↓	13	76	2.011
15	7	↓	↓	↓	15	71	1.402
16	5	↓	↓	↓	13	53	.805

*Surface entropy check failed on last line.

TABLE II.- SURFACE PRESSURE DISTRIBUTIONS

FOR TEST CASES

ϕ, deg	Surface pressure distributions for case -							
	1	2	3	4	5	6	7	8
0	---	0.9246	0.9246	0.9246	0.9241	0.9241	0.9242	0.9243
5.625	---	.9141	-----	-----	-----	.9136	-----	-----
11.250	---	.8831	-----	.8832	-----	.8826	-----	.8829
16.875	---	.8330	-----	-----	-----	.8324	-----	-----
22.500	---	.7676	.7674	.7690	.7669	.7673	.7671	.7687
28.125	---	.6894	-----	-----	-----	.6891	-----	-----
33.750	---	.6037	-----	.6013	-----	.6025	-----	.6012
39.375	---	.5148	-----	-----	-----	.5132	-----	-----
45.000	---	.4278	.4274	.4269	.4397	.4261	.4271	.4272

TABLE III.- SHOCK-LAYER THICKNESSES FOR TEST CASES

ϕ, deg	Shock-layer thicknesses for case -							
	1	2	3	4	5	6	7	8
0	---	0.1401	0.1402	0.1406	0.1407	0.1407	0.1409	0.1414
5.625	---	.1409	-----	-----	-----	.1415	-----	-----
11.250	---	.1433	-----	.1439	-----	.1440	-----	.1447
16.875	---	.1473	-----	-----	-----	.1480	-----	-----
22.500	---	.1532	.1533	.1537	.1540	.1539	.1541	.1545
28.125	---	.1614	-----	-----	-----	.1622	-----	-----
33.750	---	.1723	-----	.1730	-----	.1731	-----	.1740
39.375	---	.1863	-----	-----	-----	.1871	-----	-----
45.000	---	.2040	.2043	.2055	.2048	.2048	.2053	.2067

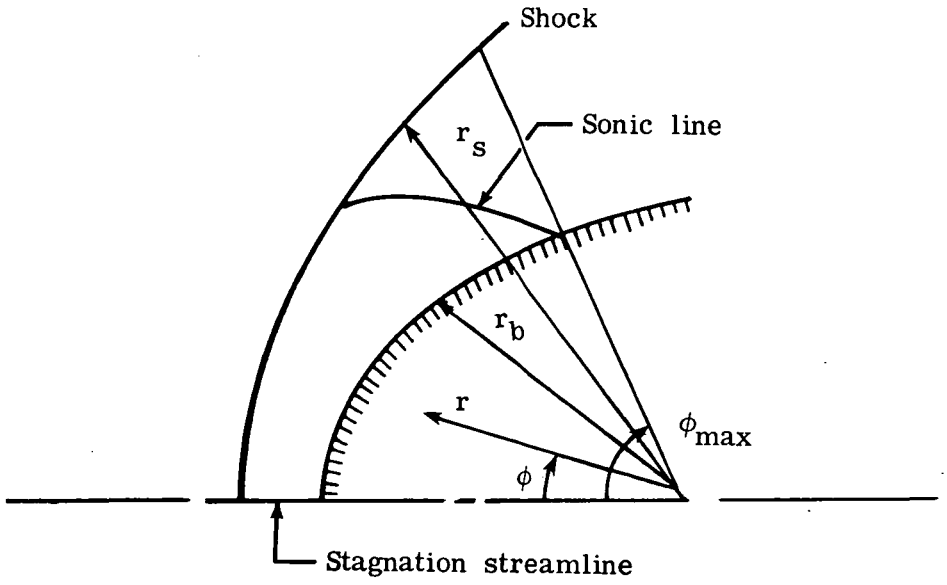

Figure 1.- Polar coordinate system.

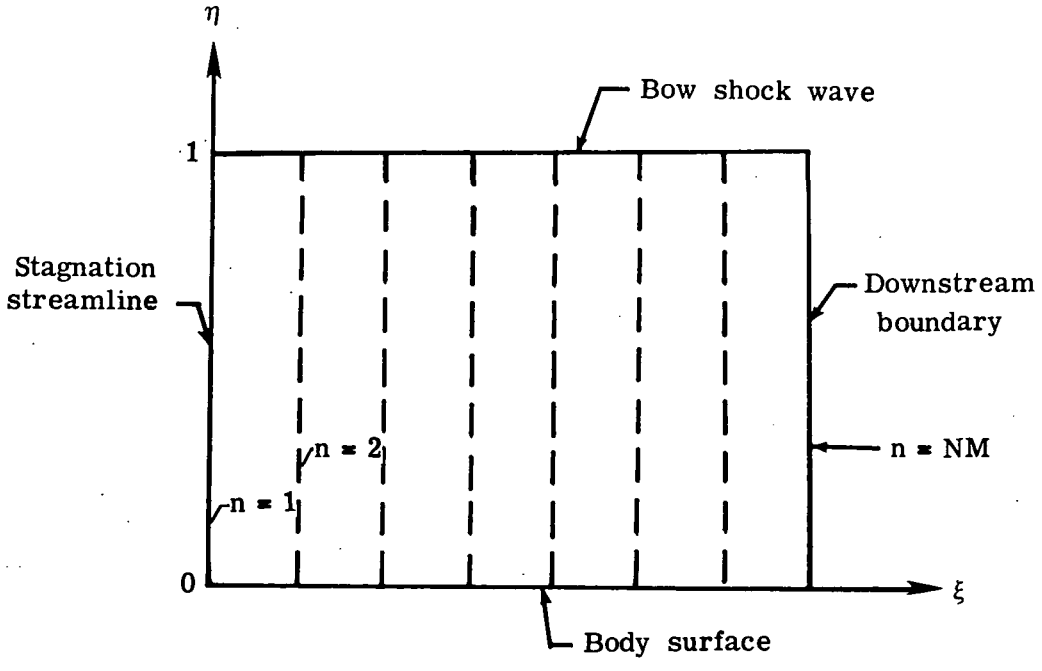

Figure 2.- Computational domain.

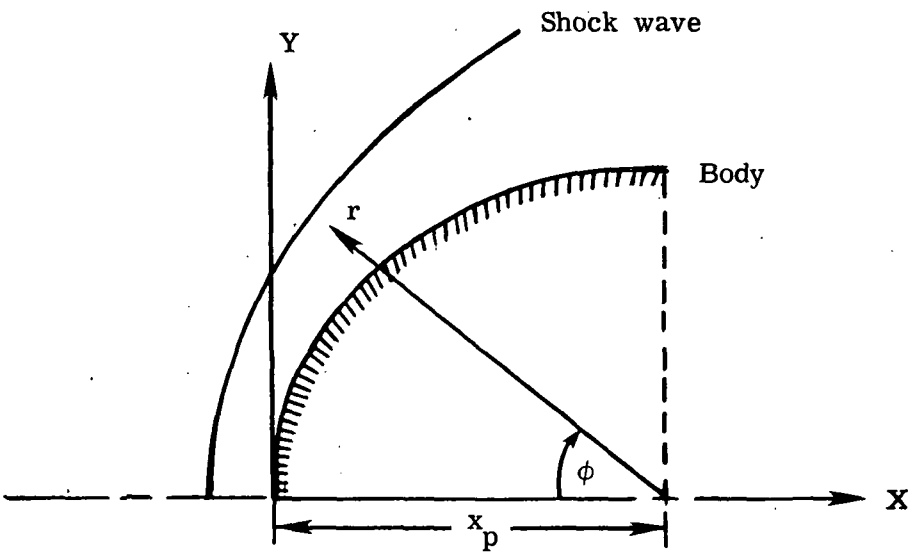

Figure 3.- Cartesian coordinate system.

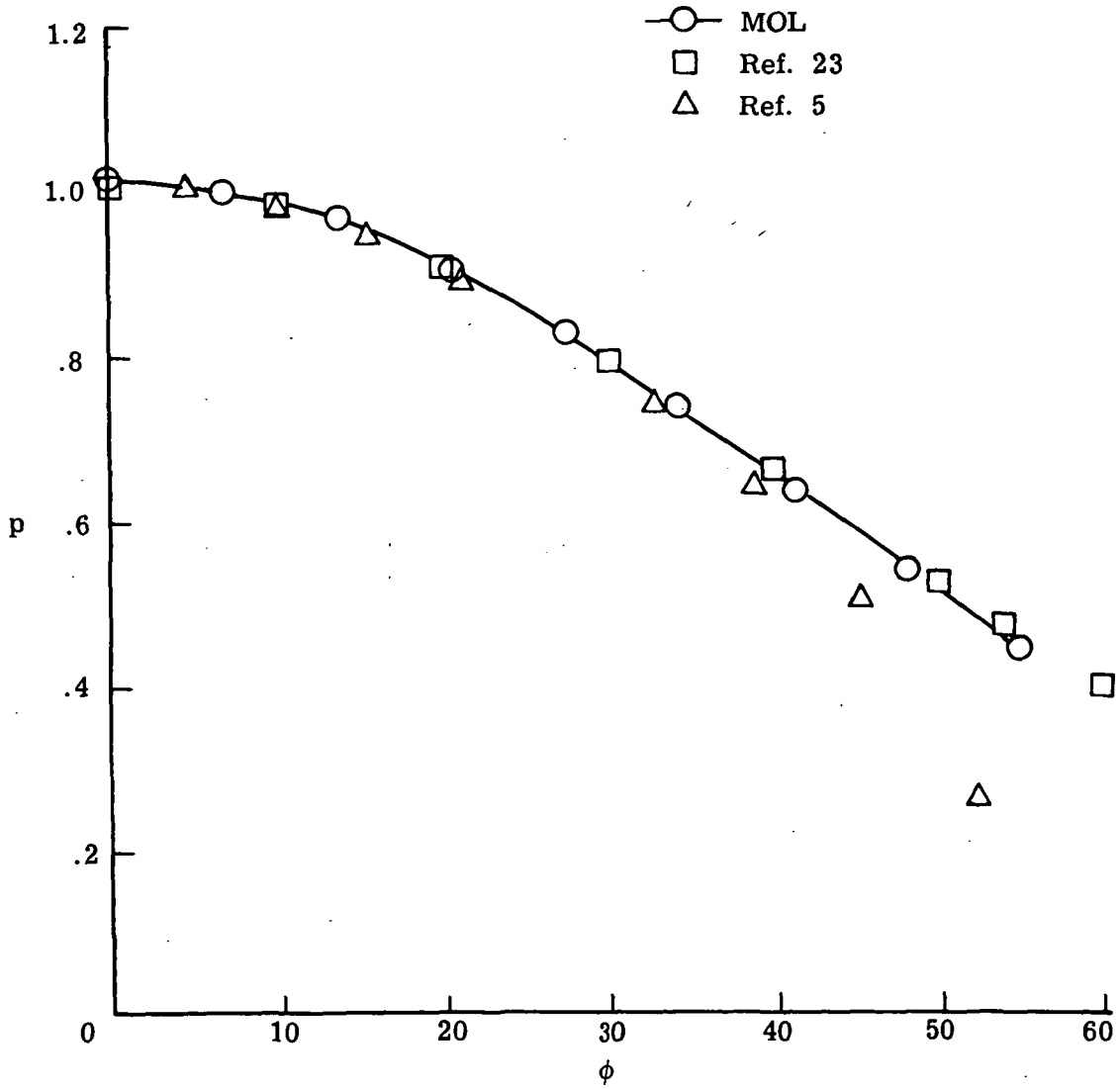

(a) $M_\infty = 2$.

Figure 4.- Pressure distribution on sphere. $\gamma = 1.4$.

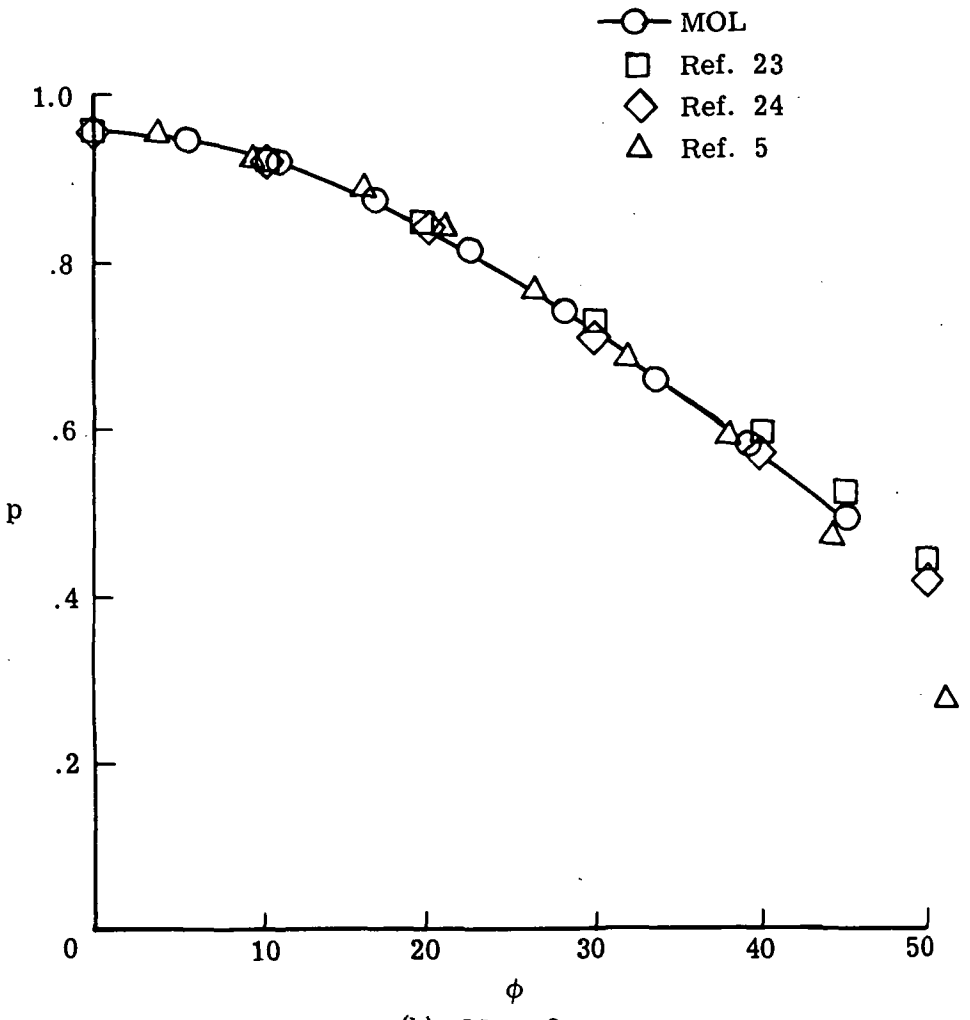

(b) $M_\infty = 3$.

Figure 4.- Continued.

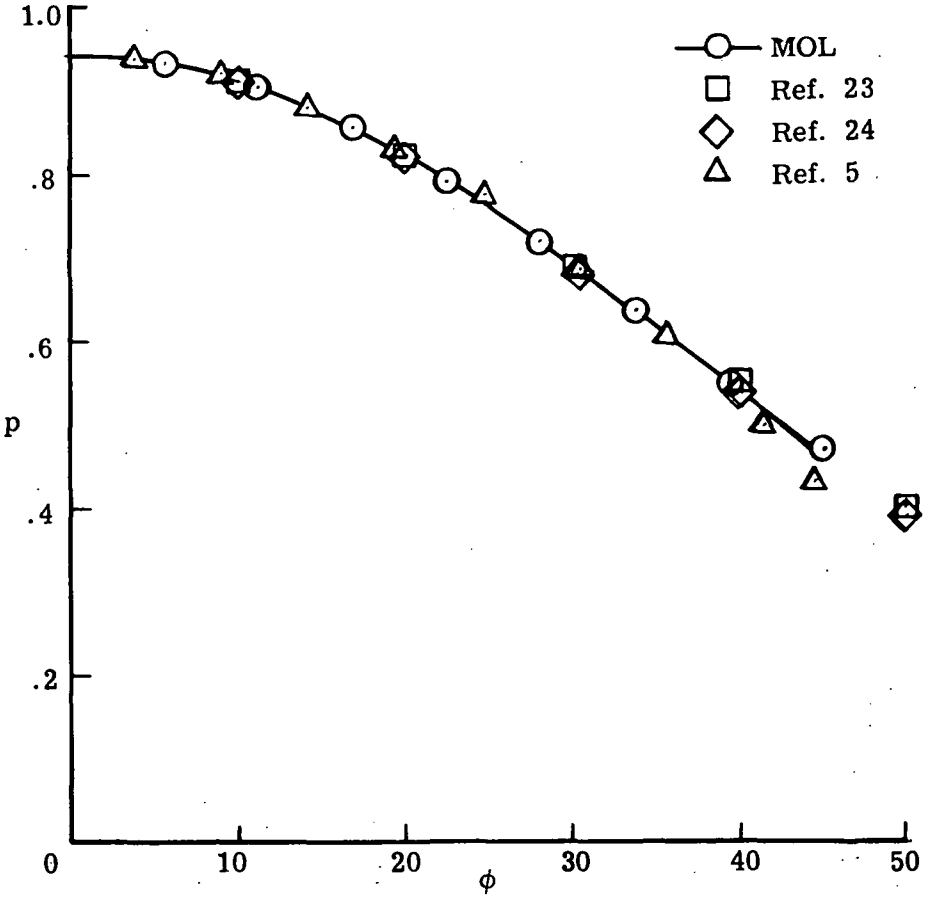

(c) $M_\infty = 4$.

Figure 4.- Continued.

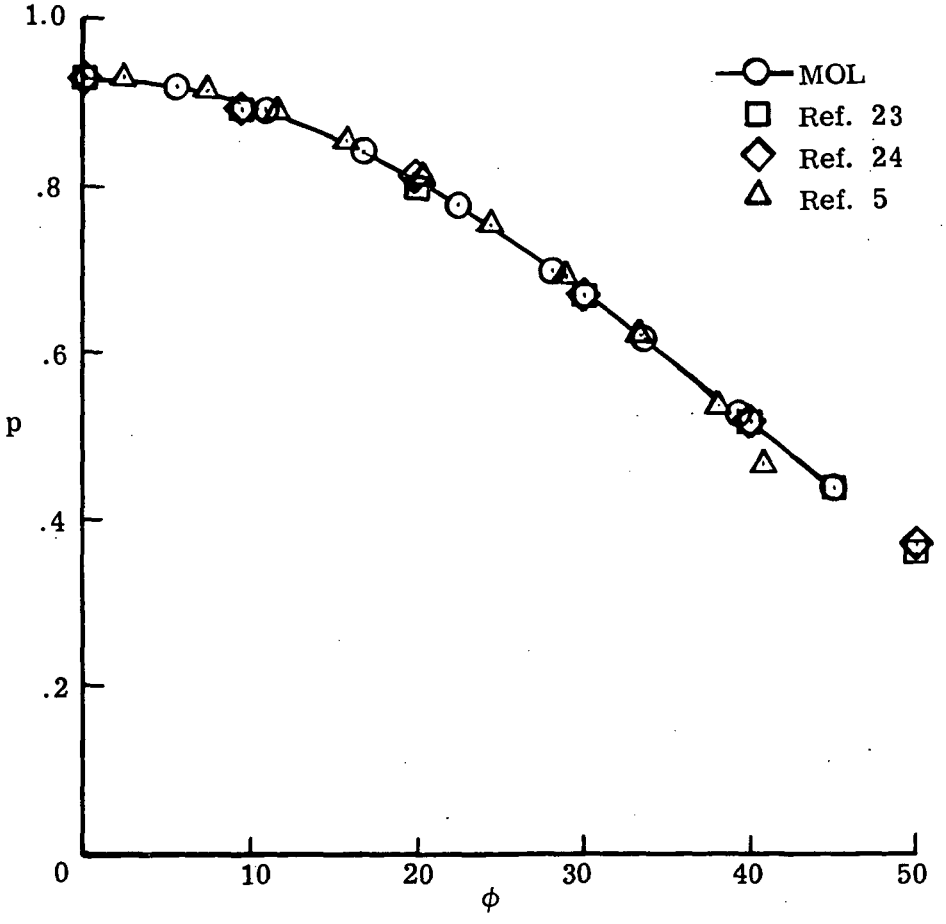

(d) $M_\infty = 6.05$.

Figure 4.- Continued.

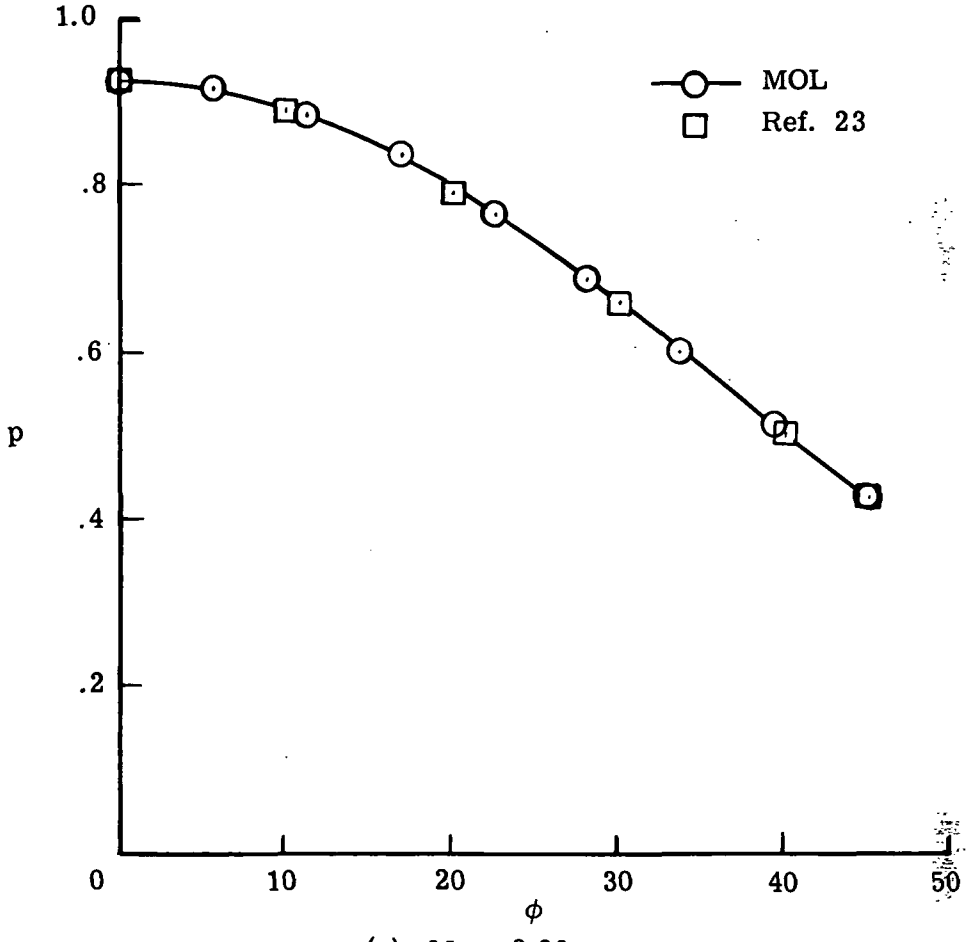

(e) $M_\infty = 8.06$.

Figure 4.- Concluded.

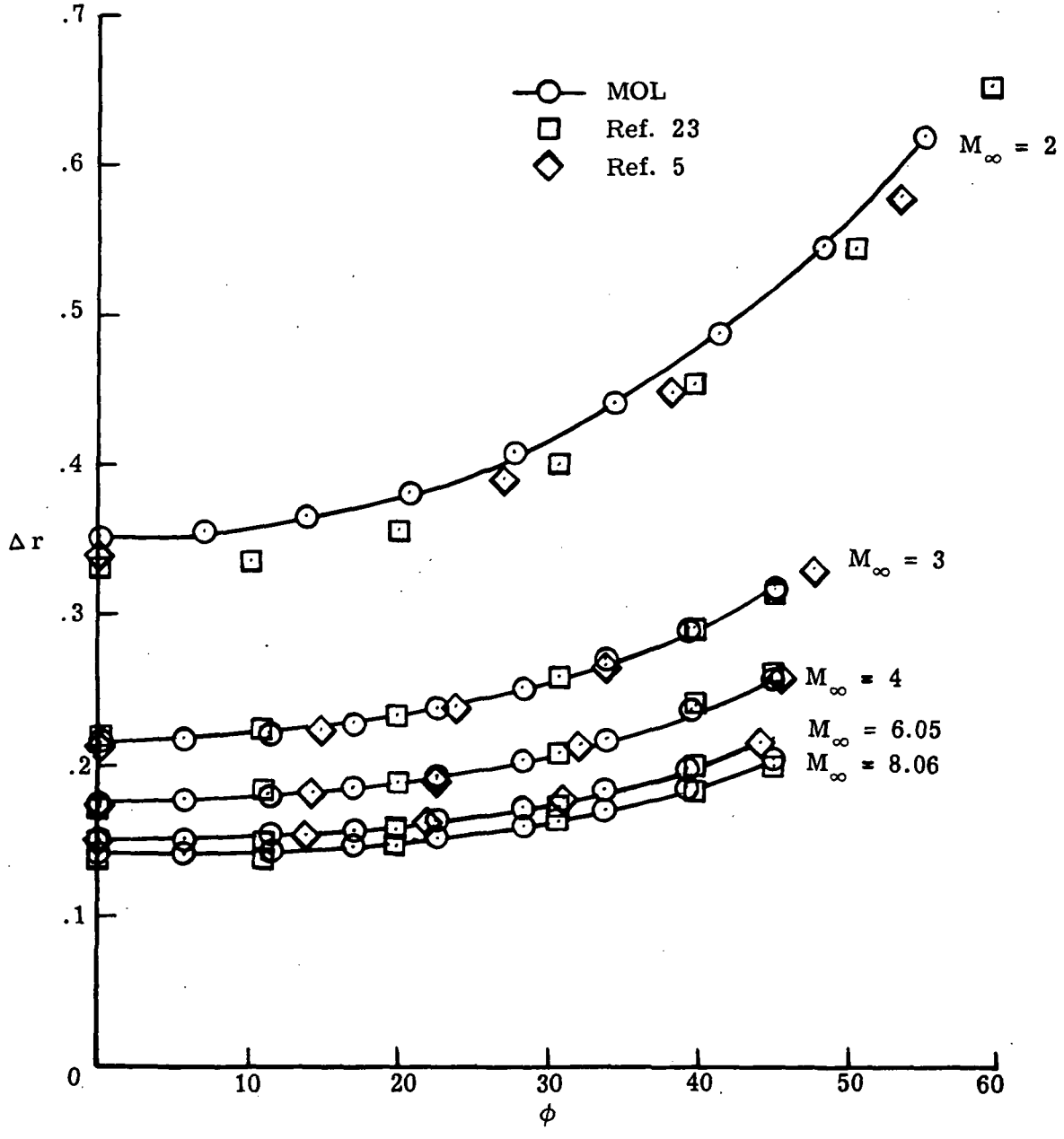

Figure 5.- Shock-layer thicknesses for sphere. $\gamma = 1.4$.

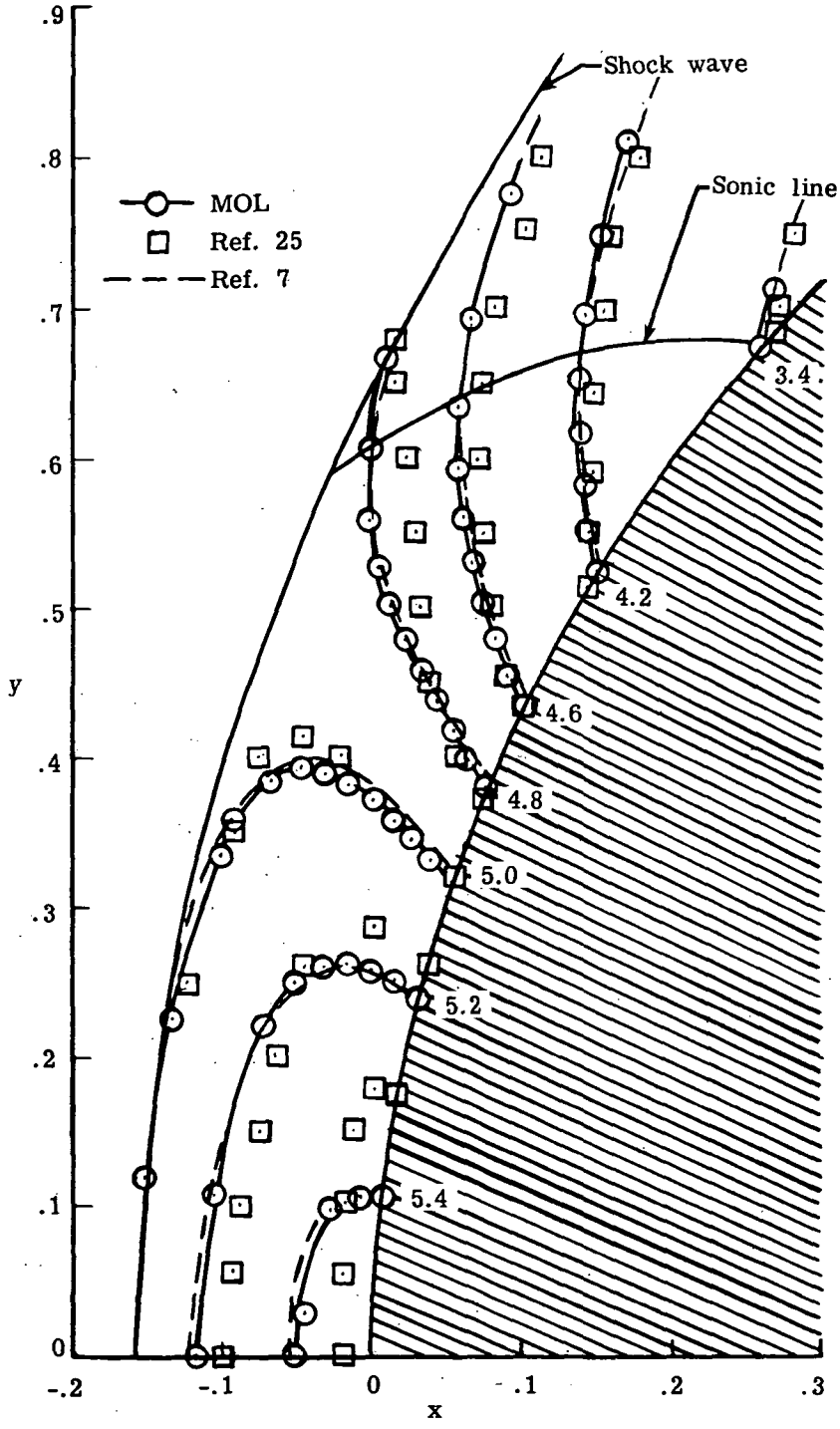

Figure 6.- Constant-density lines for a sphere in nitrogen. $M_\infty = 5.017$; $\gamma = 1.4$.

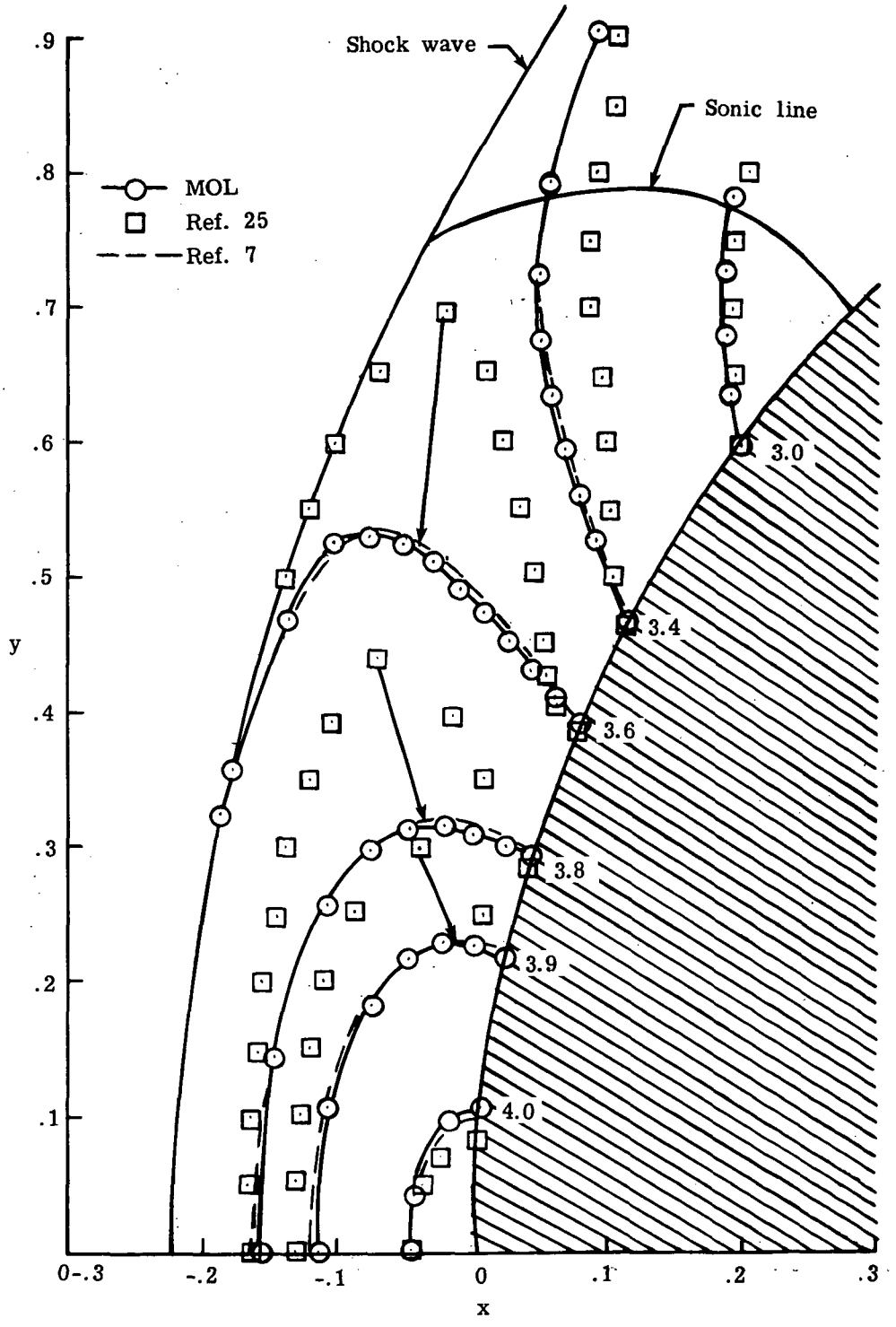

Figure 7.- Constant-density lines for a sphere in argon. $M_\infty = 5.329$; $\gamma = 1.667$.

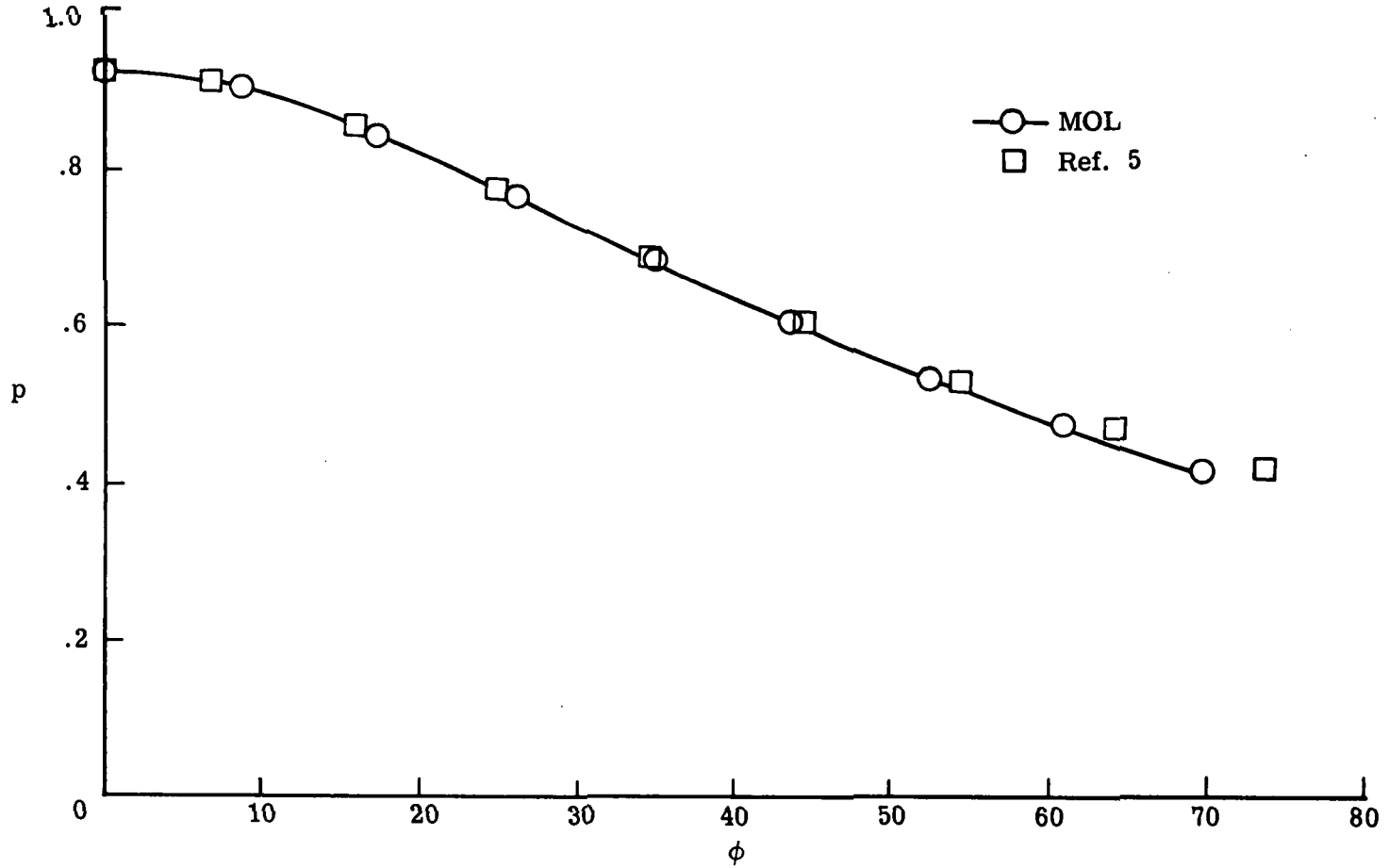

(a) $M_\infty = 10.$

Figure 8.- Pressure distribution on a paraboloid. $\gamma = 1.4$.

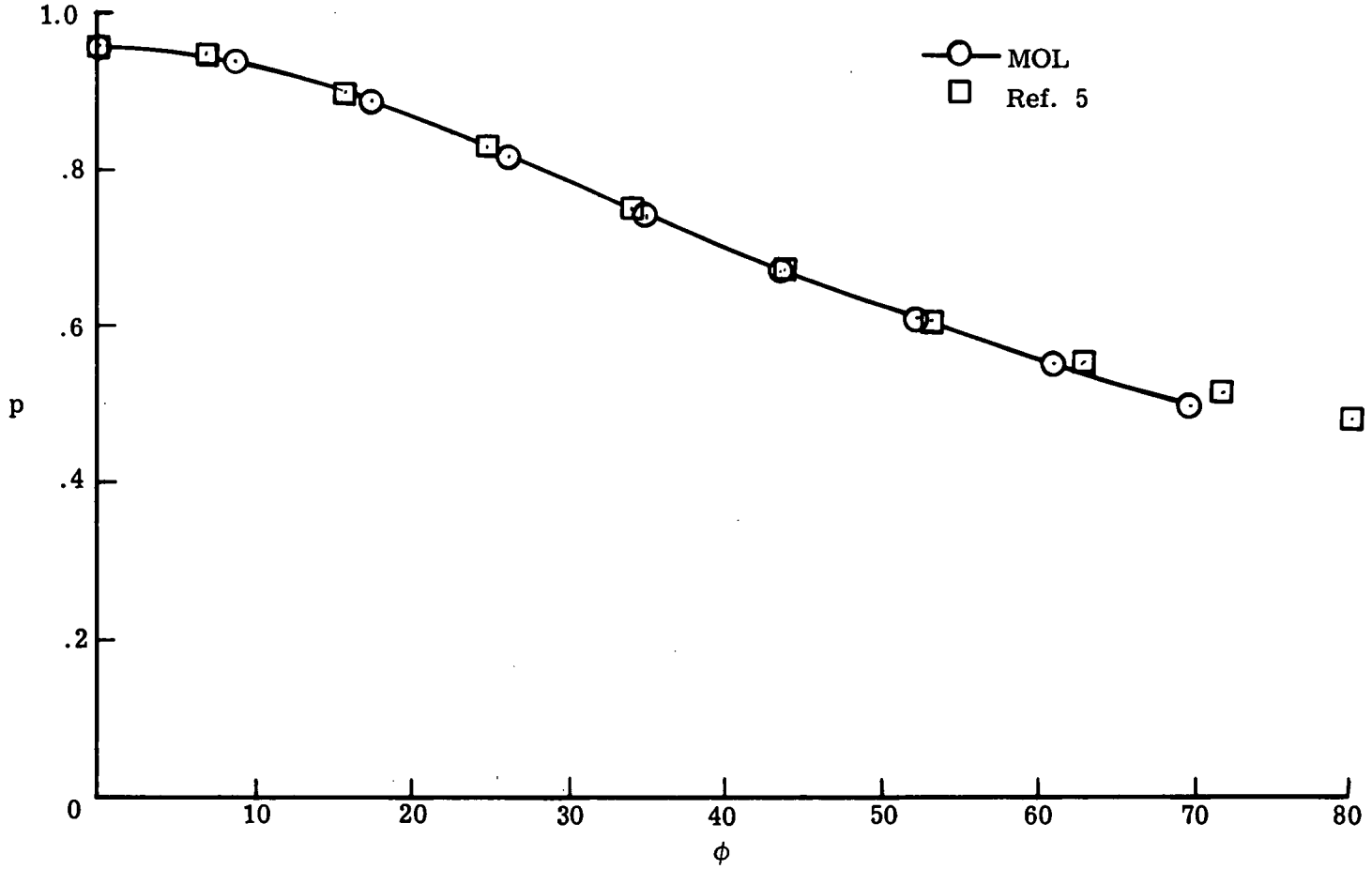

(b) $M_\infty = 3.$

Figure 8.- Concluded.

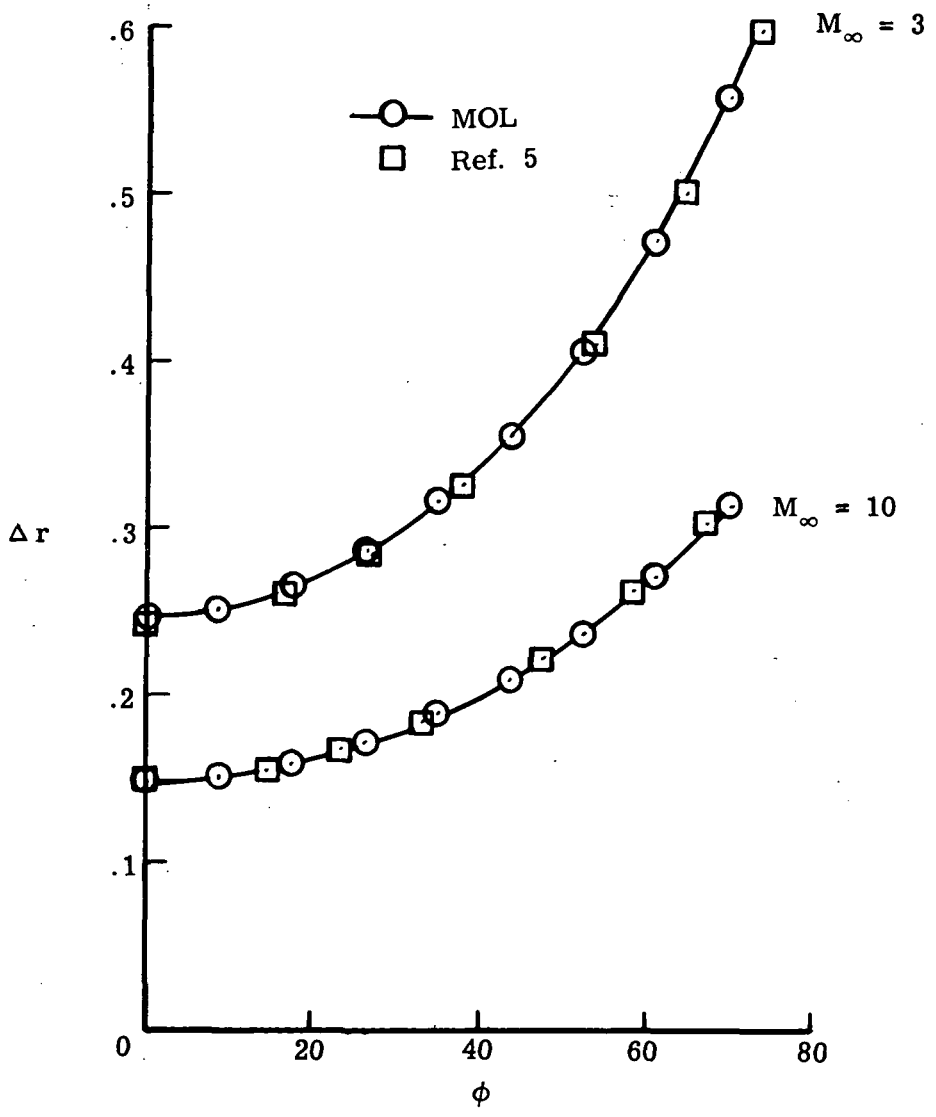

Figure 9.- Shock-layer thicknesses for paraboloid. $\gamma = 1.4$.

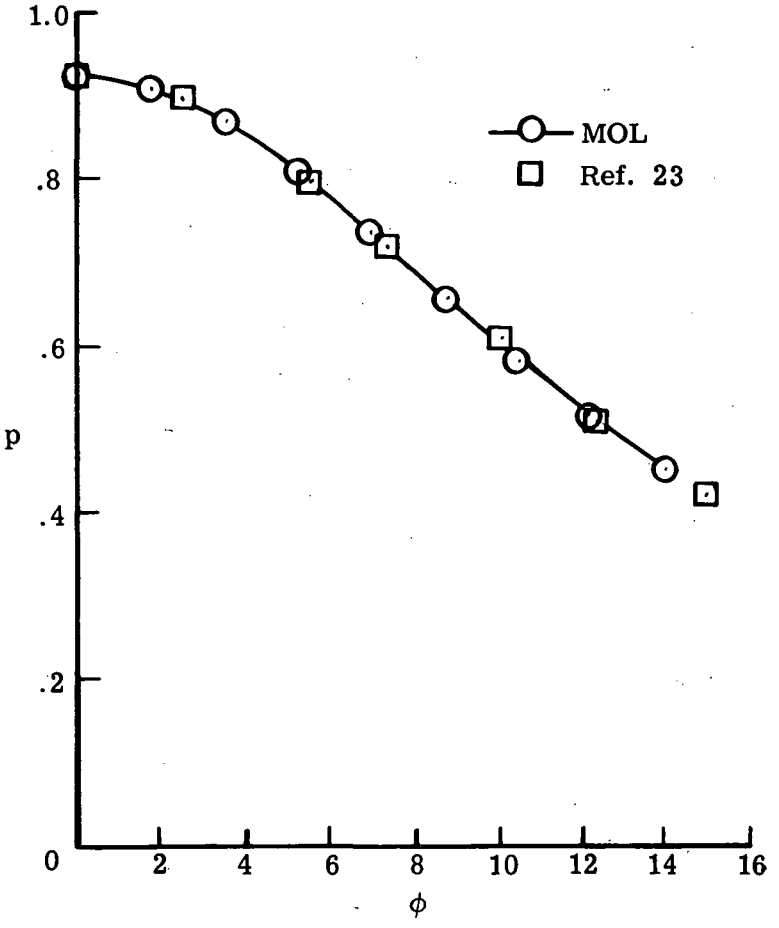

(a) $M_\infty = 8.06$.

Figure 10.- Pressure distribution on ellipsoid. $\frac{b}{a} = 0.5$; $\gamma = 1.4$.

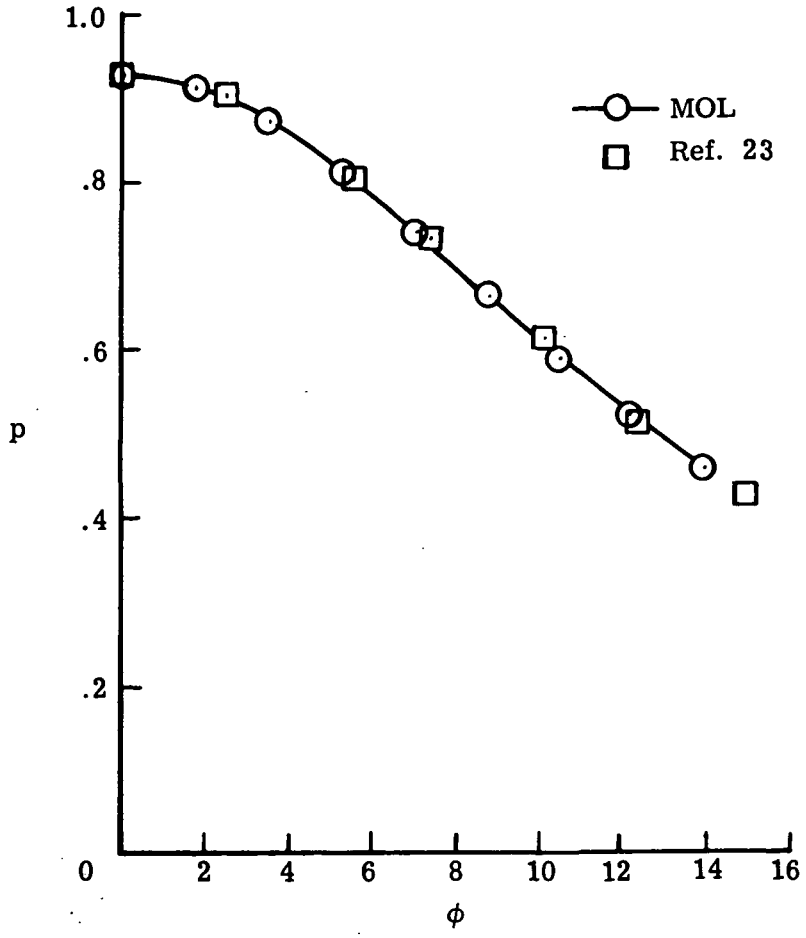

(b) $M_\infty = 6.05$.

Figure 10.- Continued.

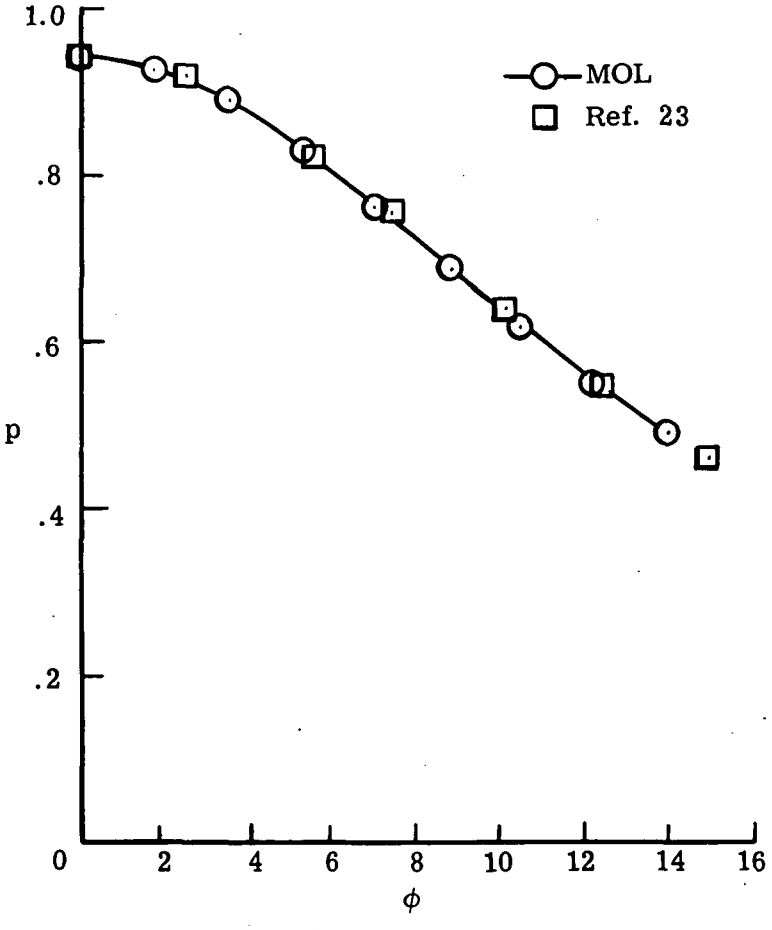

(c) $M_\infty = 4$.

Figure 10.- Concluded.

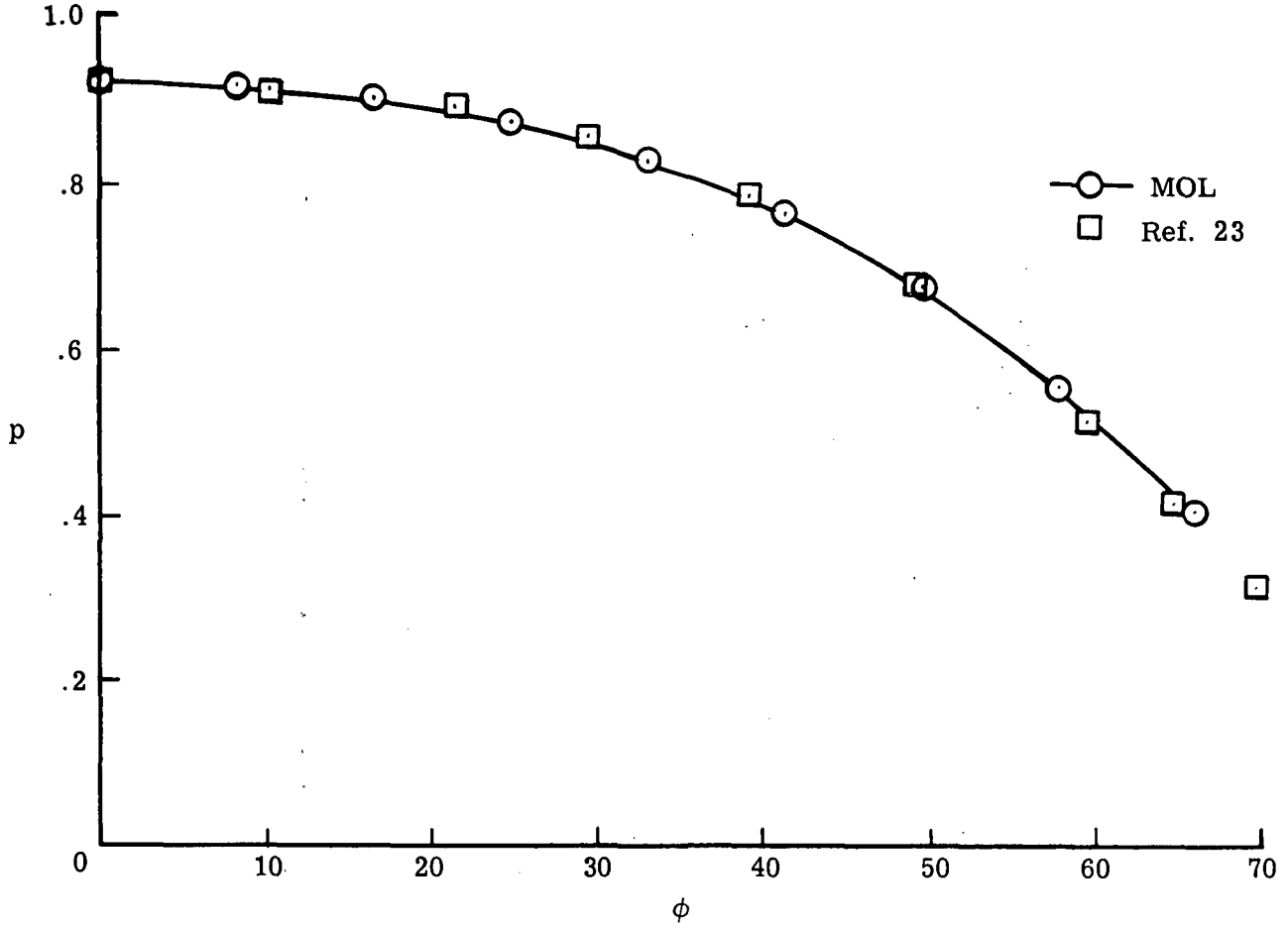

(a) $M_\infty = 8.06$.

Figure 11.- Pressure distribution on ellipsoid. $\frac{b}{a} = 1.5$; $\gamma = 1.4$.

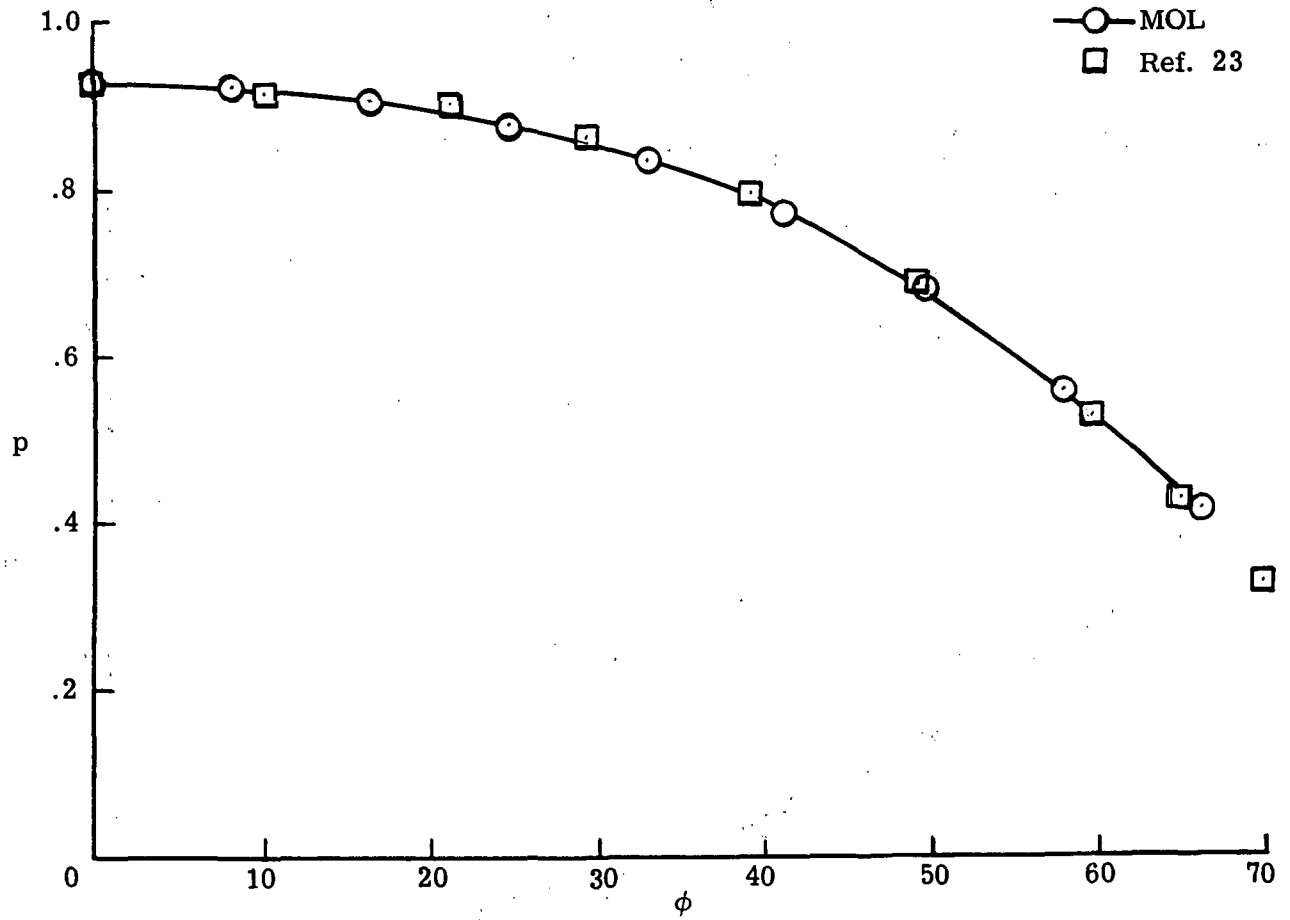

(b) $M_\infty = 6.05$.

Figure 11.- Continued.

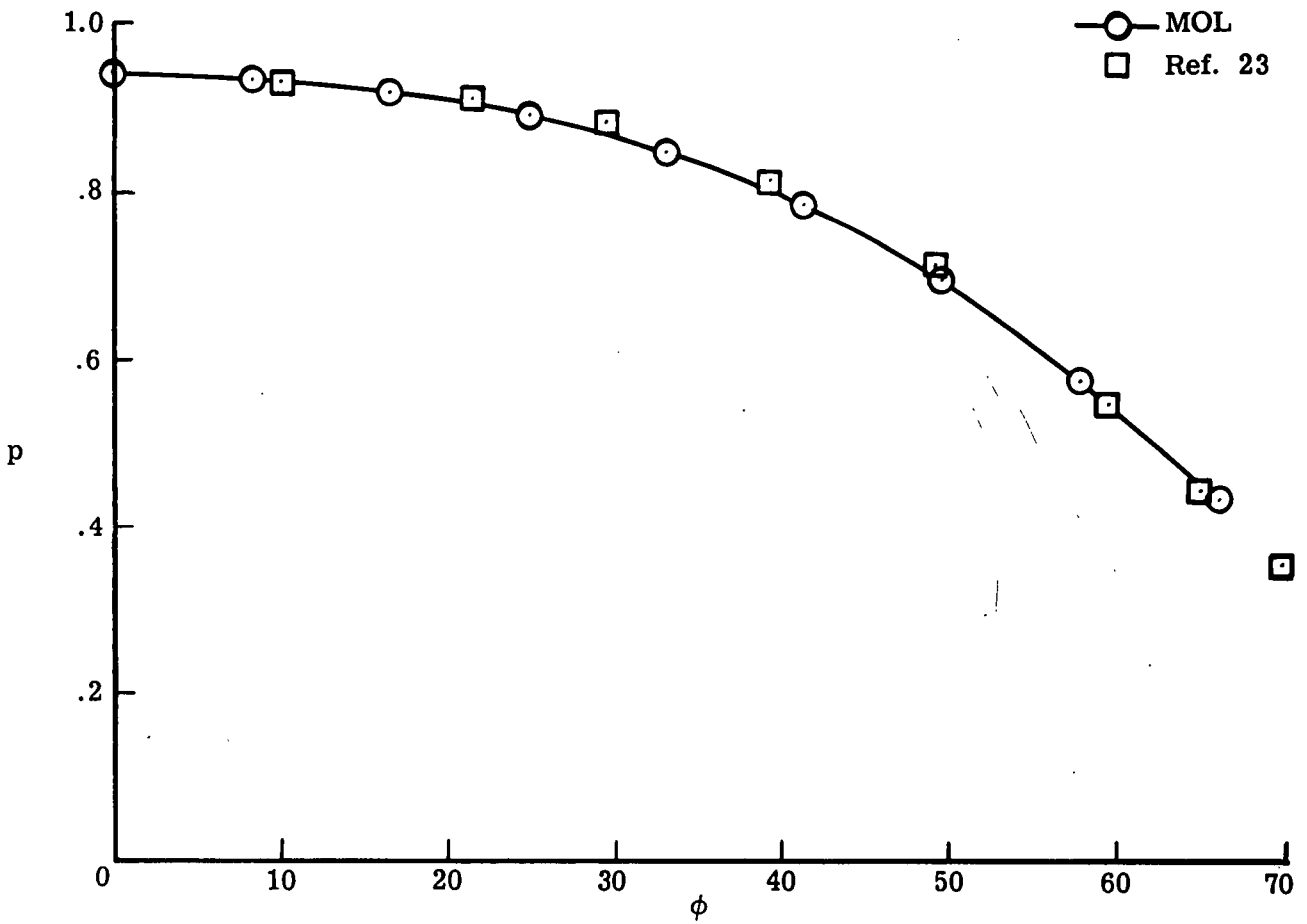

(c) $M_\infty = 4.$

Figure 11.- Continued.

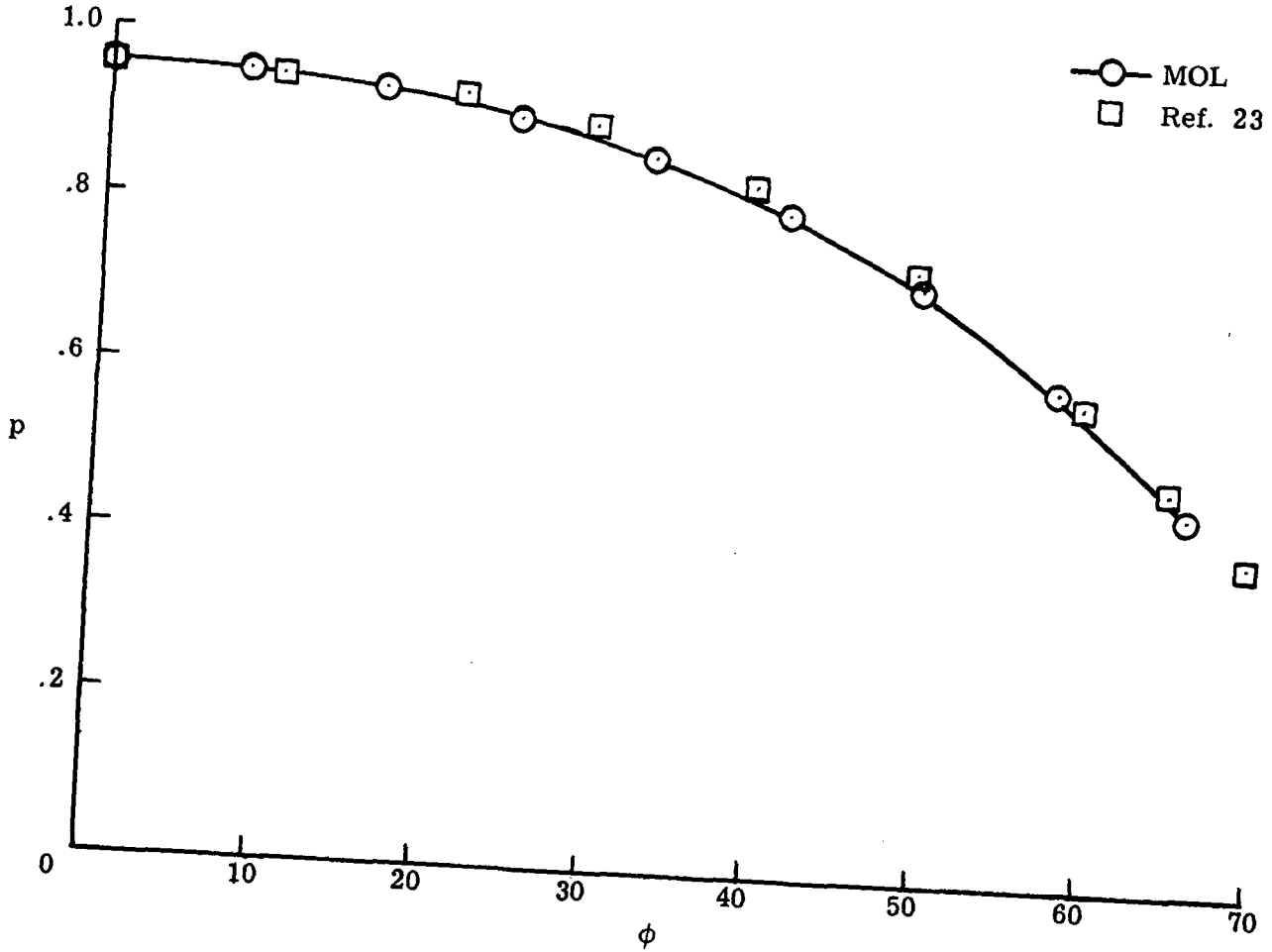

(d) $M_\infty = 3$.

Figure 11.- Concluded.

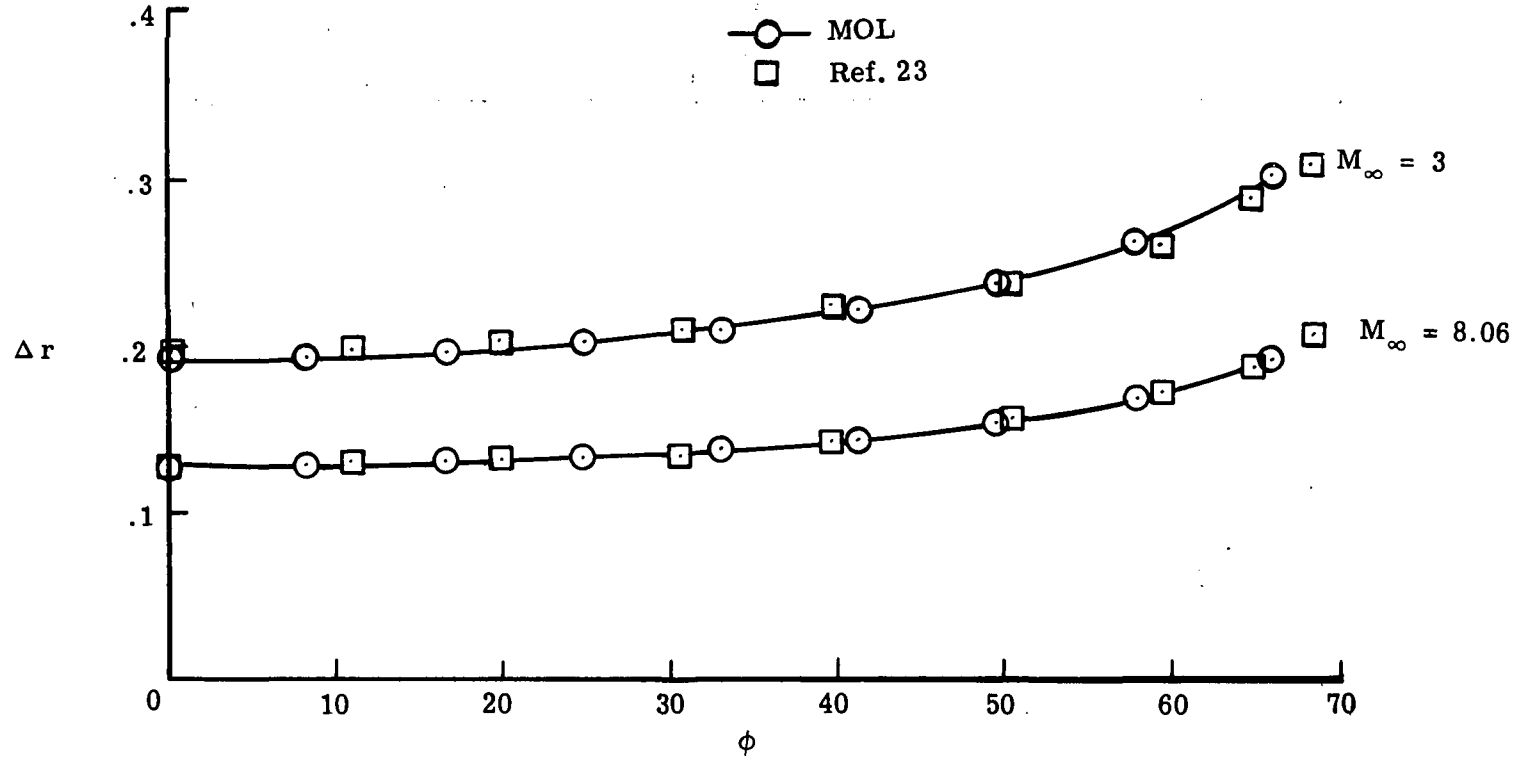

Figure 12.- Shock-layer thicknesses for ellipsoid. $\frac{b}{a} = 1.5$; $\gamma = 1.4$.

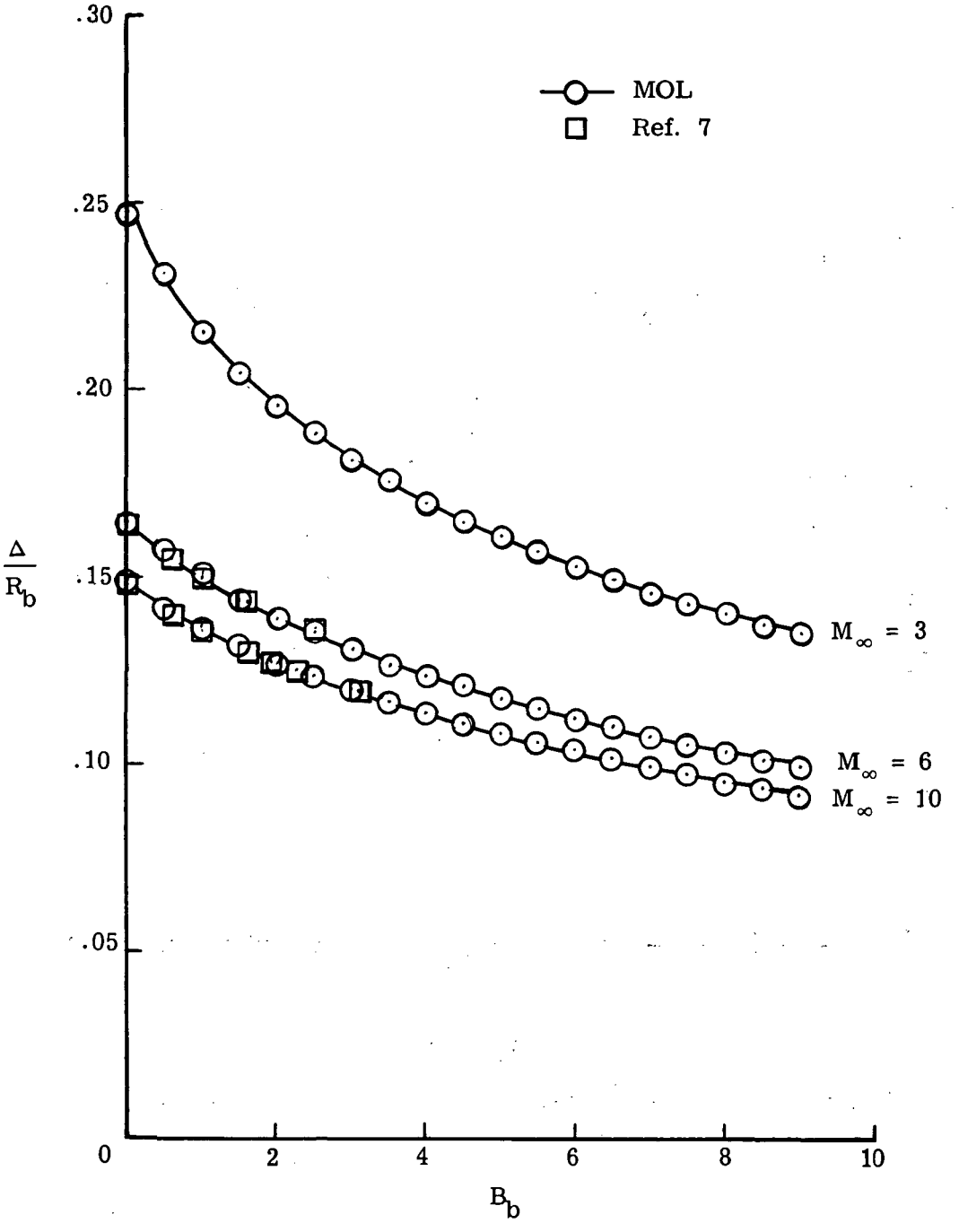

Figure 13.- Shock standoff distance for ellipsoids. $\phi = 0^{o}$.

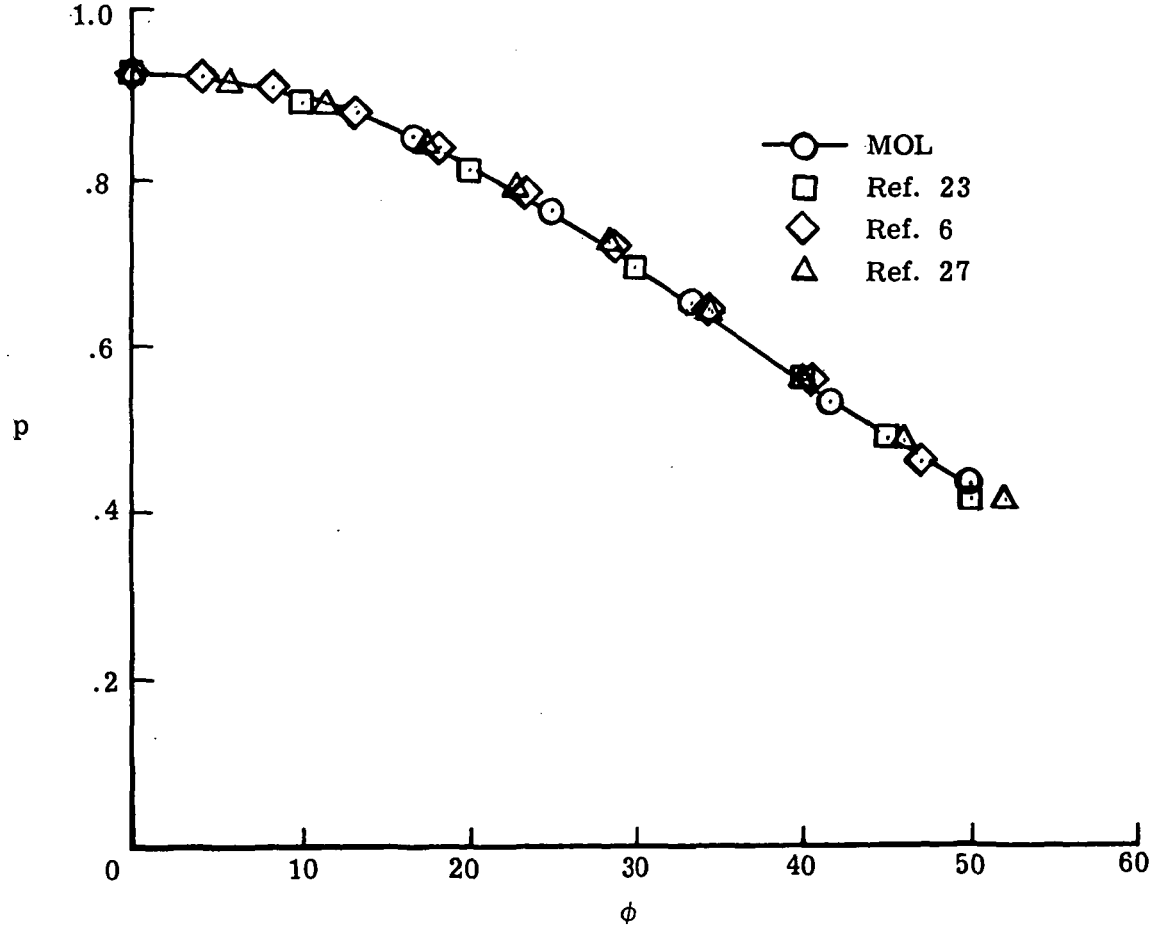

(a) $M_\infty = 8.06$.

Figure 14.- Pressure distribution for circular cylinder. $\gamma = 1.4$.

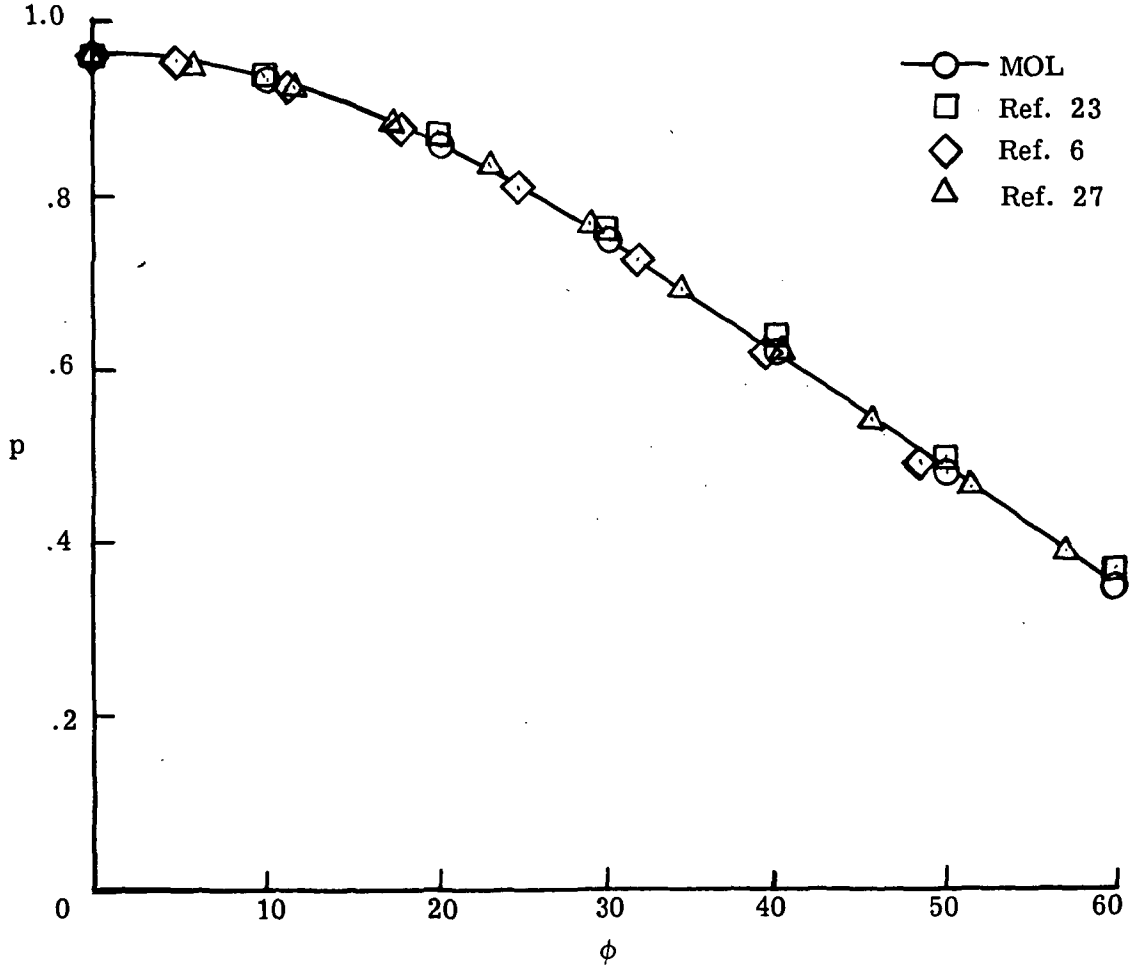

(b) $M_\infty = 3.$

Figure 14.- Concluded.

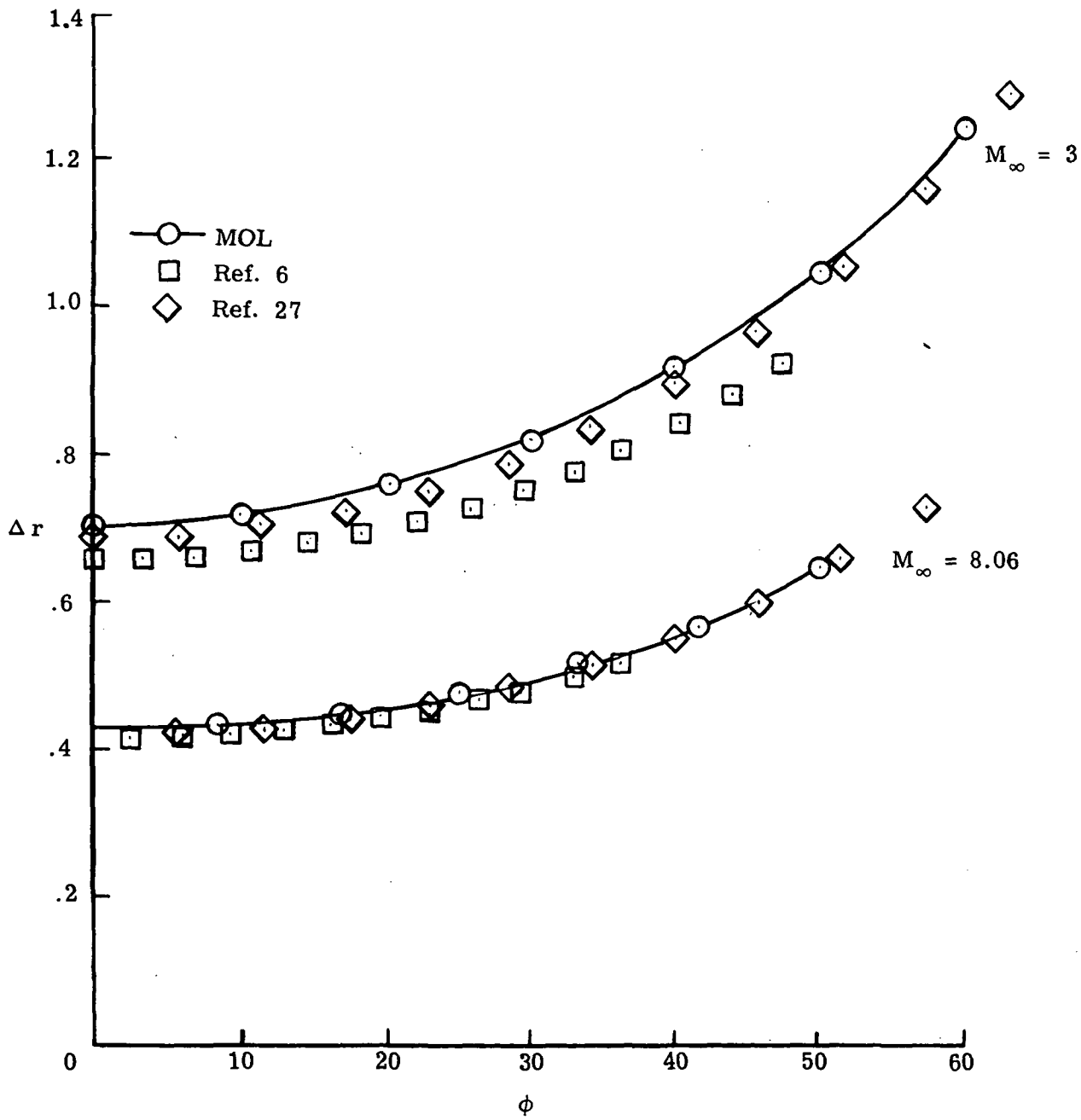

Figure 15.- Shock-layer thicknesses on circular cylinder. $\gamma = 1.4$.

1. Report No.	2. Government Accession No.	3. Recipient's Catalog No.
NASA TP-1154		

4. Title and Subtitle	5. Report Date
SOLUTION OF AXISYMMETRIC AND TWO-DIMENSIONAL INVISCID FLOW OVER BLUNT BODIES BY THE METHOD OF LINES	April 1978
	6. Performing Organization Code
7. Author(s)	8. Performing Organization Report No.
H. Harris Hamilton II	L-11983
	10. Work Unit No.
9. Performing Organization Name and Address	506-26-13-01
NASA Langley Research Center Hampton, VA 23665	11. Contract or Grant No.
	13. Type of Report and Period Covered
12. Sponsoring Agency Name and Address	Technical Paper
National Aeronautics and Space Administration Washington, DC 20546	14. Sponsoring Agency Code

15. Supplementary Notes

16. Abstract

The method of lines (MOL) has been used to obtain solutions to axisymmetric and two-dimensional inviscid flow over smooth blunt bodies. Comparisons with experimental data and the results of other computational methods have demonstrated that very accurate solutions can be obtained by using relatively few lines with this approach. The method is efficient; typical converged solutions have been obtained in 100 to 150 total integrations. The method of lines is semidiscrete and has relatively low core storage requirements as compared with fully discrete methods (such as time-dependent techniques) since very little data are stored across the shock layer. This latter feature is very attractive for three-dimensional problems because it enables computer storage requirements to be reduced by approximately an order of magnitude.

The disadvantage of the method of lines is that roundoff errors increase exponentially with number of lines; thus, the total number of lines that can be used for a particular problem is limited. In the present study it was found that 9 lines was a practical upper limit for two-dimensional and axisymmetric problems. This condition limits application of the method to smooth body geometries where relatively few lines would be adequate to describe changes in the flow variables around the body.

Extension of the method to three dimensions is conceptually straightforward; however, three-dimensional applications would also be limited to smooth body geometries although not necessarily to a total of 9 lines.

17. Key Words (Suggested by Author(s))	18. Distribution Statement
Method of lines Blunt body flows Computational fluid dynamics	Unclassified – Unlimited Subject Category 34

19. Security Classif. (of this report)	20. Security Classif. (of this page)	21. No. of Pages	22. Price*
Unclassified	Unclassified	56	$5.25

*For sale by the National Technical Information Service, Springfield, Virginia 22161

NASA-Langley, 1978

National Aeronautics and Space Administration

Washington, D.C.
20546

Official Business
Penalty for Private Use, $300

THIRD-CLASS BULK RATE

Postage and Fees Paid
National Aeronautics and
Space Administration
NASA-451

NASA

POSTMASTER: If Undeliverable (Section 158 Postal Manual) Do Not Return